8 Shear Banding in Bulk Metallic Glasses

Lan Hong Dai

State Key Laboratory of Non-linear Mechanics (LNM), Institute of Mechanics, Chinese Academy of Sciences, Beijing, China

Nomenclature

$\dot{\gamma}$ shear-strain rate
τ shear stress
T temperature
ξ free-volume concentration
D diffusion coefficient of ξ
g function is the net creation rate of ξ
k wave number
l free-volume diffusion length
$\mathbf{h}$ subscript, the homogeneous solutions
G^{ξ} $\partial g/\partial \xi$
A a constant related to the Taylor−Quinney coefficient
G^{θ} free-volume creation rate due to temperature rise
F free-volume softening
κ thermal diffusivity
Q strain hardening
R strain-rate hardening
P thermal softening
$\Gamma, \Gamma_{\mathbf{c}}$ energy dissipation in shear band and its critical value
w shear-band thickness
Ω thermal-effect coefficient
$K_{\mathbf{s}}$ shear-band toughness
G shear modulus
d STZ size
$\gamma_{\mathbf{c}}$ average shear yield strain
ν Poisson's ratio
ℓ dilatation factor
m pressure-sensitivity coefficient
$S, S_{\mathbf{cr}}$ shear-band instability index and its critical value
$\kappa_{\mathbf{M}}$ stiffness of the testing machine
E Young's modulus

d_s sample diameter
l_s sample length
L_{ext} an extrinsic length scale
L_{int} the internal resistance of a BMG to unstable shear banding
ι a dimensionless parameter accounting for the effect of machine stiffness

8.1 Introduction

Bulk metallic glasses (BMGs), due to the lack of long-range order (LRO) and the absence of traditional defects such as dislocations and grain boundaries [1−5], have a series of intriguing mechanical, physical and chemical properties [6−11]. They have shown widespread potential applications in many fields as structural and functional materials [12−16]. However, plastic flow of BMGs at room temperature (RT) is prone to be highly localized into nanoscale shear bands [17−21]. The initiation and rapid propagation of a shear band can induce catastrophic fracture with very limited ductility [22,23], impeding the further applications of BMGs. Essentially, the shear banding in BMGs is a multiple temporal−spatial and trans-scale process controlled by different physical mechanisms, during which rate-dependent processes such as viscosity/momentum diffusion, thermal/energy diffusion, free volume/mass diffusion, instability nucleation and development should be involved [19,20,24−30]. The key question is how these non-linear and coupled processes with respective characteristic time and length scales govern the shear-band formation and evolution in BMGs.

In this chapter, we present an overview of the inhomogeneous deformation behaviour of BMGs, focusing specifically on the origin (nucleation) and evolution (propagation) of shear banding. The development of BMGs as well as their atomic structure is briefly summarized, followed by an introduction to the general features of plastic flow and the underlying flow mechanisms. Then we proceed to review the results of recent research about shear banding, including experiments, continuum, atomistic modelling and theoretical developments. This chapter concludes with a summary and a view of important unresolved questions.

8.2 Development and Structure of BMGs

The existence of natural glassy materials can be traced back to around 5000 BC. However, metallic glasses or amorphous metallic alloys represent newcomers to glassy materials, having been first reported by Duwez at Caltech in 1960 [31]. Duwez's group made this discovery by rapidly quenching an Au−Si alloy at very high rates: $10^5−10^6$ K/s. The work confirmed Turnbull's prediction [32,33] that glass formation in liquid metals is possible if cooling is sufficiently fast and crystallization does not occur. Since then, greater efforts have been made to explore metallic glass systems, which exhibit a high glass-forming ability (GFA) [34−38].

As for early alloys, the timescale for crystallization was usually in the hundreds of microseconds to millisecond range. Metallic glasses were therefore formed only under very rapid solidification conditions (10^3-10^6 K/s), and they were confined to very thin sheets, ribbons or even wires with a characteristic size of less than 50 μm [39]. From the Pd-based glasses studied by Chen [40] and the Turnbull group [35] to a series of new glasses developed by the Inoue group [36,38,41], their crystallization timescales decrease significantly to the range of $1-10$ s. In particular, the Vitreloy family developed by Peker and Johnson [37] exhibits a very low critical cooling rate for glass formation of about 1 K/s. Now, a very wide range of multi-component alloys can form BMGs [7−9,14,42,43], including Pa-, Zr-, Cu-, rate earth-, Mg-, Fe-, Ti-, Ni-, Pt-based, etc. The advent of more and larger BMGs arouses a revival of interest in the basic science of glass forming, glass structure and their absorbing and potentially valuable properties [7,9−11,42,44,45].

Examination of BMGs by X-ray or electron diffraction shows the diffuse diffraction halos that may be taken as characteristic of amorphicity [46]. However, this characteristic alone is not sufficient to describe the atomic arrangements within the solid. Historically, a popular structural model for metallic glasses is that of Bernal's dense random packing of hard spheres [2,47]. The hard-sphere mode successfully describes the monatomic systems. As is well known, all BMGs are now multi-compositional, and hence their elements tend to form characteristic local atomic clusters [48]. Following the principle of the efficient filling of space, Miracle [1] proposed face-centred cubic (fcc) packing of solute-centred clusters or short-range order (SRO) as the building scheme for metallic glass structures. Such a packing mode within a medium-range order (MRO) has been confirmed by Ma and co-workers [3] using atomic simulations and directly observed by Hirata et al. [5]. Recent studies [49] suggest that over the MRO, the clusters are connected via a fractal network with the dimension of 2.31, although there are some puzzles regarding this [50]. Regions between clusters are loosely packed clusters with large free volumes [51].

Although the precise description of atomic structures for metallic glasses is still open even now, their mechanical, physical and chemical properties due to such unique structures have attracted a lasting attention. For example, they have high RT strengths much closer to the theoretical limit than their crystalline counterparts, also showing high hardness, large elastic deflection, relatively high RT fracture toughness, good wear resistance and corrosion resistance and so on [7,12]. Some Fe-based systems have excellent soft magnetic properties [52,53], and others have the capability of superconductivity [54] or hydrogen storage [55]. These strong points make them attractive candidates for potential applications ranging from defence and aerospace projects, biomedical devices and Micro Electro Mechanical systems apparatus, to communication equipment and sporting goods [7,12,13, 45,56−59]. However, BMGs have an intrinsic defect, i.e. macroscopic brittleness with very negligible RT ductility. For instance, a Zr-based BMG with substantial fracture toughness $K_{\text{IIC}} \sim 75$ MPa/m$^{1/2}$ still exhibits near-zero ductility in uni-axial tension at RT [22], as shown in Figure 8.1. Such low ductility results from the formation and rapid propagation of shear bands within samples, severely impeding
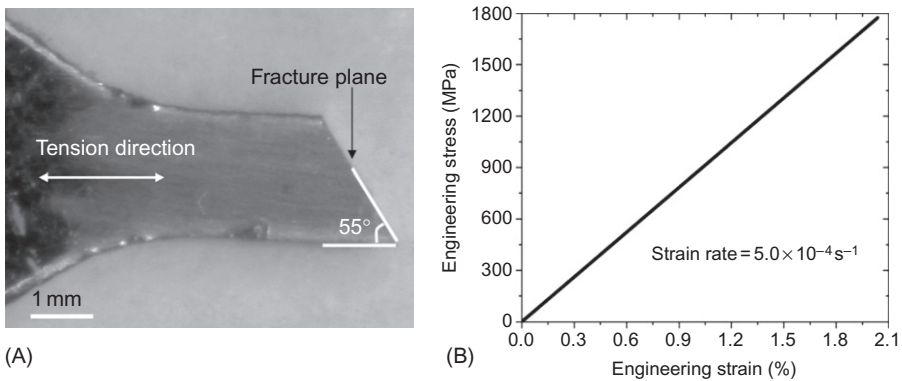
Figure 8.1 (A) Side view of the fractured sample, a Zr-based BMG, in quasi-static uni-axial tension. (B) Corresponding engineering stress−strain curve for the material.

further exploitation of this class of advanced materials. Therefore, clarifying the mechanism of initiation and propagation of shear bands is of central importance in practice. The questions of why and how a shear band with a characteristic thickness (∼10 nm) forms in an atomic-disordered medium are also interesting to scientists. Considerable efforts [10,11,19,44] have been made to examine this aspect during the past decades.

8.3   General Features of Deformation

Based on systematic examination of the deformation and fracture in metallic glasses, Spaepen [17] in his seminal paper constructed a deformation map, which draws the shear-strain rate $\dot{\gamma}$ contours with axes of shear stress τ and temperature T. The map distinguishes the plastic deformation behaviour into two basic modes: homogeneous, where each volume element of the sample contributes to the macro-scopic strain, and inhomogeneous flow, where the strain is highly localized into a few very thin shear bands. The former, due to its potential application in fabrication of micro-devices and nano-devices, has been widely studied [45,60−62]. In this chapter, the latter is our interest. The inhomogeneous flow occurs at high stresses and low temperatures. Thin shear bands are the inhomogeneous flow mode for BMGs. Figure 8.2 shows the shear-band type flow in BMGs under different loads, such as compression, shear, bending and indentation. It can be seen from this picture that in unconstrained loading geometries, e.g. tension and shear, only a few shear bands form and dominate the final failure. However, multiple shear bands can form in constrained loading modes, contributing to global plasticity of materials.

Deformation maps have recently been developed by some other researchers. Based on instrumented nano-indentation experiments, Schuh et al. [63] found that
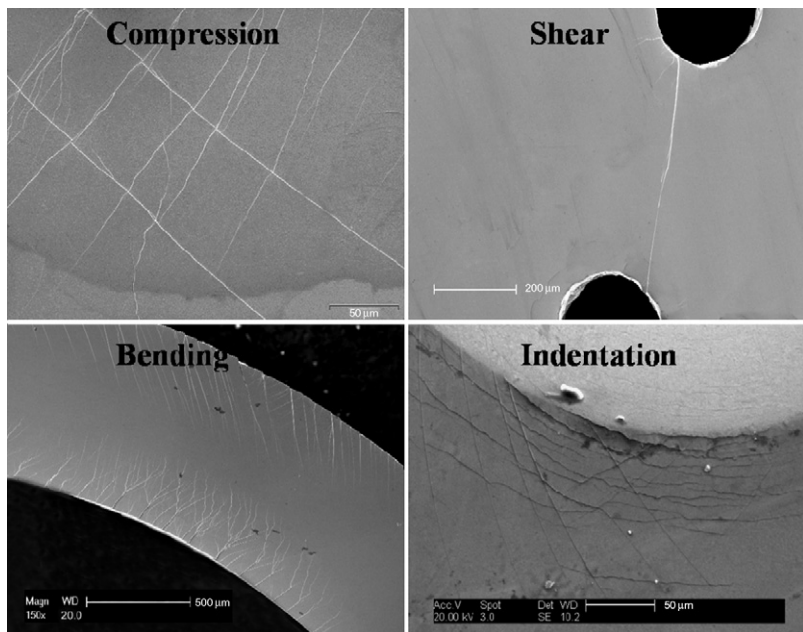
Figure 8.2 Shear bands in BMGs under different loads, including compression, shear, bending and indentation.

there exists a second homogeneous region at high-deformation rates even well below the glass transition (lying in the top-right corner of the Spaepen map). They explained that 'Homogeneous II' with no flow serrations occurs when deformation rates exceed the characteristic rate for shear-band nucleation. In fact, the disappearance of macroscopic flow serrations is mainly due to the synchronous and continued formation of many fine shear bands [64−68]. With increasing strain rates, the plastic deformation inhomogeneity tends to diminish only in time but not in space. In addition, Lee et al. [69] and Park et al. [70] recently found that BMGs can undergo homogenous deformation when they are subjected to a stress below yield at RT, held at the stress for 12 h. Such a deformation region is essentially creep flow. In particular, they observed that BMGs exhibiting more plastic strain during such homogeneous creep deformation tend to show lower global plasticity during inhomogeneous deformation. Such paradoxical phenomenon could be understood by the atomic packing density. Very recently, Furukawa and Tanaka [71] developed a novel rheological model of fracture to describe the fracture of both liquids and glasses in a unified manner. They constructed a dynamic phase diagram on the $T \sim \dot{\gamma}$ plane for a sheared, compressible viscoelastic liquid or glassy material that further divides the inhomogeneous deformation into three regions: solid-type instability, viscoelastic-type instability and liquid-type instability. This is actually consistent with the previous classification by Spaepen [17].

In general, the elastic deformation behaviour of materials is determined by the interaction of atoms inside. The plastic flow, however, should take into account the details of microstructure, more specifically defects. The flow in crystalline alloys can be described by the classical theory of plasticity underpinned by defects such as dislocations, twins or grain boundaries. These crystal defects do not exist in metallic glasses without LRO, and therefore the flow mechanism in metallic glasses must be different from that in crystalline alloys. Although the precise picture of how local atoms respond in deforming metallic glasses is not fully resolved, there is general consensus in the metallic glass community that the fundamental unit of the process underlying plastic flow must be a local *structural-rearrangement* type 'flow event' that can accommodate shear strain [17,18,72,73]. Whereas crystal dislocations allow changes in the atomic neighbourhood at low energies in crystals, the local flow event in metallic glasses requires relative high energy or high stress. Thus, how to describe such a local flow event and build a bridge between it and macroscopic deformation becomes the key to the flow mechanism.

A breakthrough has been made by Spaepen. For the first time, he applied the classical free-volume model developed by Turnbull and co-workers [74−76] to the deformation of metallic glasses [17]. Spaepen's model essentially views the flow event as an individual atomic jump. At a sufficiently high stress, an atom with a hard-sphere volume can be squeezed into a neighbouring hole with a smaller volume. This makes the neighbours of the new position move outwards and creates a certain amount of free volume. A series of discrete atomic jumps finally results in macroscopic plastic flow. The free-volume model presents a relatively systematic theoretical framework that introduces a simple state variable to the problem of glass flow. It opens a window into the understanding of the glass-flow mechanism through atomistic defects. Inspired by the shearing deformation of 2D bubble glasses [77], Argon proposed that the number of atoms involved in the flow event should be between a few to approximately 100. The flow event can be described by a local plastic or inelastic rearrangement of atoms, commonly termed the shear transformation zone (STZ). The first quantitative model of STZ behaviour was developed by Argon himself [18], who treated the problem in the context of an Eshelby-type inclusion [78,79]. He argued that an isolated STZ is not free but confined to the surrounding elastic matrix. The STZ is essentially a local cluster of atoms that undergoes an inelastic shear distortion from one relatively low energy configuration to a second such configuration, crossing an activated configuration of higher energy and volume. In a manner, an STZ in metallic glasses has an analogy with dislocation motion in crystals but at SRO length scales. Although an STZ is a flow event, not a defect, it is strongly affected by local atomic structures such as free volume, short-range chemical or topological order. For example, availability of free volume is important for the STZs to operate in a given volume of BMGs. In fact, STZ operations occur preferentially in those regions of higher free volume because relatively less dilatation is required. Spaepen [80] has envisioned that only a high free volume would contribute to deformation. He [73,80] introduced a concept of flow defect that is analogous to an STZ in terms of free volume, and he

succeeded in extending an individual atomic jump to atomic cluster rearrangement. Since Argon proposed the STZ model, scientists have made great efforts to capture such flow events via experiment or simulation [72,81,82].

Either the free-volume or the STZ model is a mean-field theory. Nevertheless, the two models provide a basis for further analysis of the strain localization process in BMGs. Following the STZ model, Johnson and Samwer [83] made the first attempt to deal with such an aspect. They proposed a cooperative shear model (CSM) to understand the yield strength when inhomogeneous deformation occurs, although the spatial features of inhomogeneous deformation were still precluded in their analysis. As mentioned earlier, an isolated STZ is always confined by the surrounding elastic medium. Such elastic confinement would lead to reversible elastic energy storage in the STZ-matrix system, implying that transformed STZs have a memory of their original untransformed state. A question naturally arises: How do these STZs with memory induce memoryless plastic flow? Johnson and Samwer [83], Mayr [84] and Harmon et al. [85] argued that this process is analogous to a relaxation mechanism of glasses, which can be explained from a potential energy landscape (PEL) perspective [86−88]. The individual STZ operations can be viewed as fast β-relaxation processes that are sub-IS hopping events. The avalanche percolation of these STZs is associated with the slower α relaxation process, an intra-IS hopping event. The plastic irreversible α hopping event will contribute to macroscopically perceptive plasticity. The CSM model thus suggested that inhomogeneous yielding occurs when a critical fraction of 'minimum' barrier STZs becomes unstable and results in global instability. Merging this picture with the Frenkel model [89] of shear strengths in dislocation free solids, Johnson and Samwer [83] derived a universal power law of two-thirds of temperature for the yield strength of metallic glasses. Based on the CSM, the activation energy and size of STZs have been determined by simulations [84] or experiments [81]. Very recently, Yu et al. [90] provided possible evidence that the activation of STZs and β-relaxations are directly related by examining their activation energies.

8.4   Physical Origin of Shear-Banding Instability

The flow theories reviewed in the preceding material successfully explain how a metallic glass deforms plastically; however, these theories do not give a clear answer to inhomogeneous deformation or shear banding. Why does the flow in a metallic glass localize into such extremely thin shear-band regions? What initiates this localization process? What is the onset condition of shear-banding instability? These questions continue to plague and challenge scientists. Historically, there are two hypotheses as to why shear bands occur in metallic glasses. The first suggests that shear-induced dilatation inherent in the flow event causes the generation and coalescence of free volume, leading to a precipitous drop in viscosity within the shear band. This idea originated from the work of Spaepen [17]. Subsequent works from Argon [18], Steif et al. [91], Vakes [92], Falk and Langer [72], Huang et al. [24] and Wright et al. [93] have also shown the importance of free-volume dynamics

to shear instability. Here, the free-volume formation is indeed a stress-drive structural change; hence, this hypothesis contends that shear banding in metallic glasses has a structural origin. Alternatively, Leamy et al. [94] proposed that shear-banding events are thermally initiated, similar to adiabatic shear bands (ASBs) in crystalline alloys. Local adiabatic heating occurs, decreasing the viscosity by several orders of magnitude within the shear band. Although the two concepts seem contradictory, in both cases, a change in viscosity localizes the deformation and incurs shear banding. Actually, based on systematic experimental and theoretical investigations [25,26,28,30,95−97], Dai and co-workers [19,20,27] proposed that the free-volume creation joining with the temperature rise induces the shear-band initiation in metallic glasses. In this coupled softening process, however, the free-volume softening plays the dominant role, while the thermal softening is the assistant effect. To clarify the third hypothesis, it is necessary to reinspect the shear bands in metallic glasses, especially focusing on variables that affect their origin.

8.4.1 *Variables Relevant to Shear Banding*

The most noticeable feature of shear bands in metallic glasses is that they can form at low (usually quasi-static) strain rates, whereas ASBs in crystalline alloys usually occur in dynamic cases. In addition, shear bands in metallic glasses also exhibit strain-rate dependence. To investigate whether the strain rate exerts a role in the shear-band formation in BMGs, Dai and co-workers [25,28,96] performed different strain-rate levels of plate shear, shear-punch and compressive testing on BMG specimens. Figure 8.3 shows the shear-band patterns (arrow point) at the notch tip during plate shear. The number of shear bands is smaller at quasi-static strain rates (Figure 8.3A) than that at dynamic strain rates (Figure 8.3B). The spatially positive strain-rate dependence of shear-banding formation is also clearly observed in the shear-punch tests, as shown in Figure 8.4. This figure shows that the number density of shear bands (arrow point) around the circular deformation region at dynamic strain rates (Figure 8.4B) is far larger than that at quasi-static cases (Figure 8.4A). This trend seems to be consistent with a series of otherwise experimental observations, such as tensile testing by Mukaia
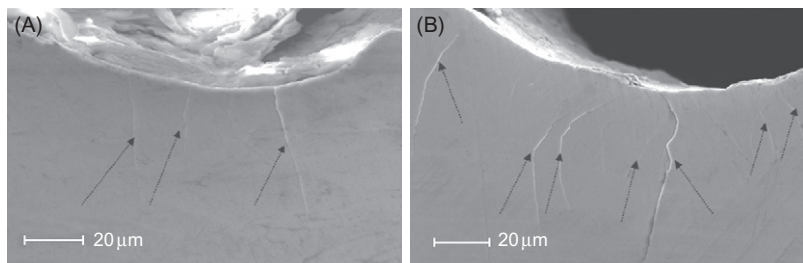

Figure 8.3 Shear-band patterns at the notch tip in Vit 1 BMG under (A) quasi-static and (B) dynamic plate shear.
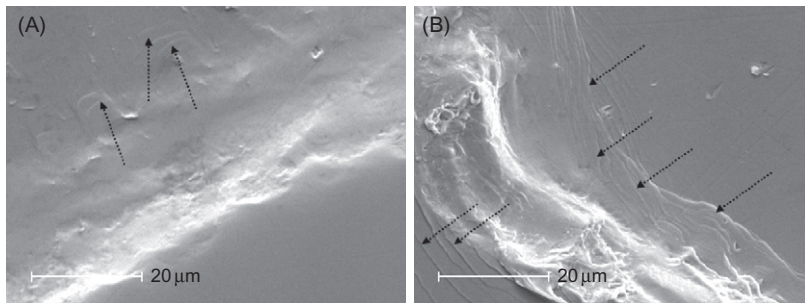
Figure 8.4 Shear-band patterns around the circular deformation region in Vit 1 BMG during shear punch under (A) quasi-static strain and (B) dynamic rates.

et al. [98], compressive testing by Jiang et al. [22] and indentation by Dai et al. [95] and Subhash and Zhang [65]. Recently, Jiang et al. [68] performed compression tests on Zr-based BMGs at various strain rates. They indeed observed that, with increasing strain rate, shear bands tend to form continuously in time. In other words, a higher strain rate promotes shear-band formation. However, the resultant spatial patterns can be of positive or negative effects, depending on material components and stress states. The strain-rate dependence on spatio-temporal features of shear banding implies that momentum dissipation plays an important role on the shear-banding process.

The characteristic thickness of mature shear bands (MSBs) in metallic glasses also attracts much attention by providing an important clue to their origin. Masumoto and Maddin [99], perhaps for the first time, reported deformation lines (shear bands) with a thickness of 20 nm on the tension side of the sample, during bending of a filament of $Pd_{80}Si_{20}$ metallic glass. Later, precise measurements showed a narrow range of thicknesses, listed in Table 8.1, identifying 10 nm as the characteristic thickness of shear bands in metallic glasses. It is impossible for such extremely localized flow to be thermal induced (discussed shortly) because atomic/cluster-scale structural changes should be responsible for it. For example, Pampillo [107] found that the shear bands were preferentially etched. Similar preferential attack phenomenon was also noticed by Donovan and Stobbs [100] in the deformation of an Fe-based metallic glass ribbon, and recently by Dai and co-workers [26] in the pre-etching sample surfaces, as shown in Figure 8.5. The preferential etching susceptibility of these shear bands clearly means that the chemical potential within the bands has been changed with respect to the rest of the materials. These researchers believed that it is the structural change that leads to this effect by destroying the SRO structure existent in metallic glasses to a more disordered structure. In fact, such disordered structures correspond to the free-volume defect, which was confirmed by work carried out by Li and Li [108,109], Gu et al.[104], Chen et al. [105], Cao et al. [110] and Flores et al. [111]. In particular, Donovan and Stobbs observed enhanced small-angle scattering in the shear bands formed in tension, which they attributed to the presence of sub-nanometre-scale voids. They speculated that excess free volume, stabilized by shear stress during deformation,

Table 8.1 Summary of Measurements of Shear-Band Thickness in Metallic Glasses

Metallic Glass (in at%)	Method	Thickness (nm)	Observers
$Pd_{80}Si_{20}$	TEM of replica	20	Masumoto and Maddin [99]
$Fe_{40}Ni_{40}B_{20}$	TEM	$10-20$	Donovan and Stobbs [100]
$Zr_{56.3}Ti_{13.8}Cu_{6.9}Ni_{5.6}Nb_{5.0}Be_{12.5}$	TEM	≤ 10	Pekarskaya et al. [101]
$Zr_{57}Ti_5Cu_{20}Ni_8Al_{10}$	HRTEM	≤ 20	Li et al. [102]
$Al_{90}Fe_5Gd_5$; $Al_{86.8}Ni_{3.7}Y_{9.5}$	HRTEM	$10-15$	Jiang and Atzmon [103]
$Zr_{52.5}Ti_{17.9}Cu_{20}Ni_8Al_{10}$	HRTEM	~ 15	Gu et al. [104]
$Zr_{65}Al_{7.5}Ni_{10}Cu_{7.5}Ag_{10}$	HRTEM	~ 5	Chen et al. [105]
$Cu_{47.5}Zr_{47.5}Al_5$	HRTEM	~ 10	Kim et al. [106]
$Zr_{41.2}Ti_{13.8}Cu_{10}Ni_{12.5}Be_{22.5}$	AFM	~ 20	Jiang and Dai [30]

TEM, transmission electron microscopy; HRTEM, high-resolution TEM; AFM, atomic force microscopy.
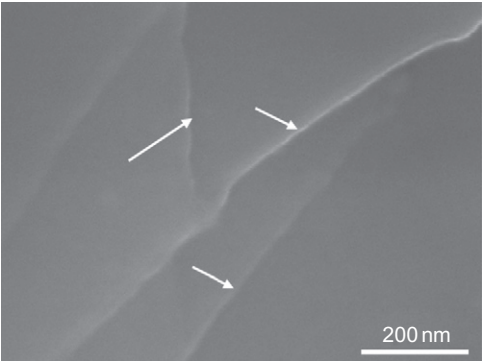

Figure 8.5 Preferential etching at shear bands in a Vit 1 BMG.

coalesced into voids after the deformation stopped. Dai and co-workers [26] did observe some nanovoids (Figure 8.6) formed at the intersection sites of the shear bands in a post-deformed Vit 1 BMG. These experimental phenomena − including the preferential etching of shear bands, excess free volume within shear bands and nanovoids at the intersection sites of shear bands after deformation − provide useful information that local structural changes occupy a unique niche during the initiation of shear bands in metallic glasses.

Shear bands, as a form of localized plastic flow, are not completely free from the thermal effect or local heating. Shear bands in metallic glasses are no exception either. Indirect evidence for local heating comes from melted droplets on the fracture surface (Figure 8.7) or a sparking phenomenon at the moment of fracture. However, it is incorrect to deduce that shear bands in metallic glasses have a thermal origin or are essentially an adiabatic phenomenon, especially at their initiation stage. One way to approach this question is to attempt to calculate the temperature
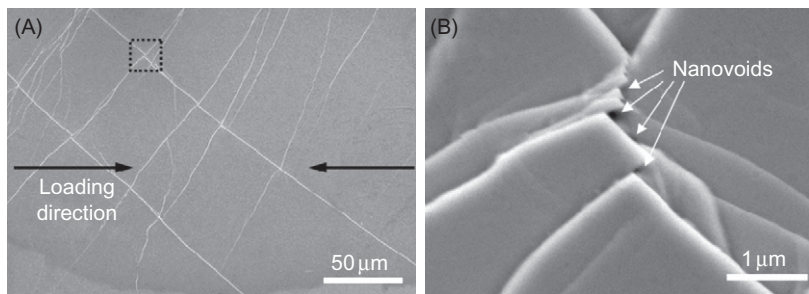
Figure 8.6 (A) Multiple shear bands formed during quasi-static compression of a Vit 1 BMG and (B) nanovoids exist at the intersection site of shear bands indicated in (A).
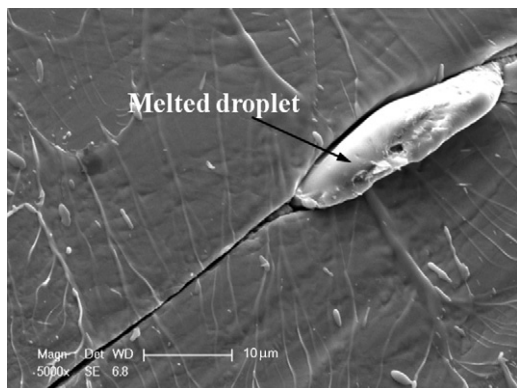

Figure 8.7 Melted droplet on tension fracture surfaces of a Zr-based BMG.

rise within a shear band. The reasonable calculation requires a precondition that we must know the mode of shear-band propagation or, more specifically, the shear-band velocity. It can be deduced that as the shear-band velocity increases, the predicted maximum temperature increases because less time is available for thermal dissipation away from the shear band. The shear-band velocity in metallic glasses has values ranging from 10^{-5} m/s to a few km/s. The calculated maximum temperature in shear band therefore varies from tens of kelvin to several thousand degrees kelvin [25,39,112−116], leading to confusions. It is well known that the most powerful evidence of whether the local heating occurs during shear banding or not is gained by directly measuring temperature rise in shear bands, which is hindered by the extremely thin thickness and short duration of shear bands, however [117−121]. Recently, Lewandowski and Greer [115] invented a clever, simple way to improve the resolution of measurements. They coated a Vit 1 BMG with a thin layer of tin and observed it after double-notched, four-point bending. This method has remarkable resolution: 30 ps (the thermal diffusion time through the coating) and 100 nm (the scale of the melting bead of the coating), respectively. Based on the observations of many melted hemispherical beads of a thin deposit at the notch that underwent shear banding, and further treating shear bands as planar sources of

heat, they reported that the temperature rise in the shear band may be several thousand degrees. However, it is noted that their estimation strongly depends on the duration of shear banding (they adopted 90% of the shear-wave speed). In addition, shear bands were observed by Zhang et al. [122], which did not incur melting of the tin. Recently, by revising the shear time and stress for an operating shear band, Miracle et al. [116] recalculated the thermal profiles around the band and concluded that the temperature rises were insignificant. In fact, according to the ex situ observation, we do not exclude such a possibility that the melting of the tin occurs during the final fracture event. Notwithstanding a lot of controversy, the local heating, maybe as an accompanying effect, remains important to shear banding in metallic glasses [123].

As we know, shear banding is a dissipation system. ASBs in crystalline solids are determined by the competition between the momentum dissipation and the energy (heating) dissipation. The preceding review of experimental observations demonstrates that strain rate, free volume and local heating are all possible factors affecting the shear-banding instability in metallic glasses.

8.4.2 Continuum Modelling and Analysis

Argon [18] modelled the flow localization (shear band) as a consequence of strain softening from the free-volume clustering. He considered a shear band located in the centre of a 1D planar layer initially shearing at a constant strain rate. Then, he introduced the free-volume dynamics into the constitutive equations that are described within the STZ formulism; he further derived a bifurcation equation describing the divergence of strain rate in and out of the band. His numerical solutions show the strain acceleration in the band with increasing applied shear strain and the concomitant decrease of shear-strain rate in the surrounding matrix. A similar analysis was performed by Steif et al. [91], via developing Spaepen's free-volume model [17]. He derived the constitutive and free-volume evolution equations for the band and the matrix, respectively. In this case, the free-volume perturbation in the band was introduced directly. Calculations showed that such perturbations can indeed cause the shear-strain localization in the perturbation zone.

Later, Spaepen's free-volume mode was generalized by Steif et al. [124], and Huang et al. [24] added multi-axial stress states through the use of the Mises stress τ_e or the effective stress. In particular, Huang et al. [24] introduced the free-volume diffusion into the free-volume evolution process. The diffusion of the free volume is analogous to the diffusion of vacancies in crystalline materials. Thus, the free-volume evolution equation becomes

$$\frac{\partial \xi}{\partial t} = D \frac{\partial^2 \xi}{\partial y^2} + g(\xi, \tau_e) \tag{8.1}$$

where the g function is the net creation rate of free-volume concentration ξ, including the free-volume generation and annihilation [17], and D is the diffusion coefficient of

the free-volume concentration. By linear stability analysis for homogeneous flow, Huang et al. revealed that the homogeneous flow will become inhomogeneous if the net generation rate of free volume is greater than its diffusion rate, i.e.

$$\frac{\partial g}{\partial \xi} > k^2 l^2 \qquad (8.2)$$

where k is the wave number of the perturbations and l is the free-volume diffusion length scale. Further calculation indicated that, with the applied shear strain under simple shear, there is a peak in $\partial g/\partial \xi$ that corresponds to a stability point due to the free-volume coalescence. Such a physical picture was recently re-examined by Gao [125] who developed an implicit finite-element method (FEM).

   All the results just mentioned lend insight into the free-volume origin of shear bands in metallic glasses. However, these analyses exclude the thermal effect. In other words, the shear-band formation is considered as an isothermal process. Recently, Gao et al. [29] performed a thermo-mechanical instability analysis of a shear band in metallic glasses, through the introduction of the thermal transport equation into the free-volume-based constitutive law. In contrast to the result of Huang et al. [24], they revealed that an increase in temperature perturbation brings about the bifurcation from homogeneous to inhomogeneous deformation modes. In fact, the thermal instability only plays a secondary role in the shear-band instability, which will be discussed shortly.

   Since we proposed in 2005 for the first time [27] the coupled effect of free-volume softening and thermal softening on shear-banding instability, it has been identified by more and more work [126−130]. However, some critical questions have not been answered well. During such a coupled process, is either free-volume softening or thermal softening responsible for the onset of shear instability? How do the free volume and temperature interplay with each other, and how do they act? Recently, Dai and co-workers [19,20,27] presented a theoretical description of coupled thermo-mechanical deformation of BMG undergoing a 1D simple shear, focusing on the physical origin of shear-band instability. Considering that the strain rates, the free volume and the temperature rise are possible factors in initiating a shear band, their model takes into account the momentum balance, the energy balance and the dynamics of the free volume, during which the constitutive law can be the same as Steif et al. [91] and Huang et al. [24]. Firstly, they examined the homogeneous deformation case. By defining the thermal instability index and the free-volume instability index, they revealed that the free-volume production facilitates the sudden increase in the temperature before instability and vice versa. Through a rigorous linear perturbation analysis, they obtain the onset condition for a shear-band instability (subscript 'h' denotes the homogeneous solutions) [20],

$$G_{\mathrm{h}}^{\xi} + \frac{A\tau_{\mathrm{h}} G_{\mathrm{h}}^{\theta} F_{\mathrm{h}} - \kappa Q_{\mathrm{h}} k^2}{\kappa R_{\mathrm{h}} k^2 + Q_{\mathrm{h}} - A\tau_{\mathrm{h}} P_{\mathrm{h}}} > Dk^2 \qquad (8.3)$$

where the left side denotes the net generation rate of free volume that is temperature dependent and the right side is its diffusion rate. Obviously, this criterion, Eq. (8.3), is physically analogous to the condition in Eq. (8.2), but the difference is that the former involves the temperature effect. Actually, if the free-volume softening dominates, the criterion in Eq. (8.3) can totally reduce to the condition in Eq. (8.2) proposed by Huang et al. [24]. If the shear instability is dominated only by the thermal softening under the adiabatic limit, the criterion in Eq. (8.3) is identical to the onset condition for the conventional thermoplastic shear instability revealed by Bai [131]. According to the instability condition in Eq. (8.3), the dynamic balance between the stabilizing and destabilizing effects determines a critical wavelength. By examining the dominant instability mode, we can obtain the internal timescale in the present coupling-softening instability. According to the relative importance of the free-volume softening and thermal softening, the internal scales can be converted into the internal free volume or thermal scales, respectively.

The internal length scale measures whether the instability occurs easily or not, while the internal timescale characterizes how fast the instability initiates. The internal length and timescales are plotted against the applied strain rates in Figure 8.8. Clearly, the internal scales of instability for the three cases decrease with increasing strain rate. This might be the main reason that the shear instability due to either thermal softening or free-volume creation is more probable at higher strain rates. This numerical result agrees well with the available experimental observations [25,28,95]. The internal free-volume length and timescales are remarkably smaller than those in the thermal-softening case, indicating that shear instability resulting from free-volume creation occurs easier and faster than thermal instability. At low strain rates, the thermal internal length and timescales are very large. This implies that thermal softening occurs with great difficulty at low strain rates. However, at this strain rate, the free-volume softening still appears. It is well known that shear banding instability in BMGs occurs not only at high strain rates but also at quasi-static loading, as described in Section 8.4.1. So, it is probable that shear banding or strain localization is started by free-volume softening. This weak influence of thermal softening on shear instability at low strain rates results in, the coupling shear-instability behaviour are more like that due to free-volume creation. In such cases, shear instability in BMGs approaches an isothermal process, during which the internal length scale is approximately tens of nanometres, and the internal timescale is roughly the inverse of strain rate. As the strain rate increases to the dynamic range, such as 10^3 s^{-1}, the internal length scales due to both free-volume softening and couple softening decrease to nanometres or sub-nanometres, while the thermal length scale is of the order of $10-100 \text{ μm}$. Also, the coupling of softening with the internal timescale ($\sim$μs) occurs much faster than the sole thermal-softening timescale ($\sim$ms). Therefore, under a dynamic strain rate, the thermal softening favours the shear instability originating from free-volume softening, leading to lower values of internal length and timescales in the coupled softening case.

Furthermore, a shear-band analysis similar to those by Argon [18] and Steif et al. [91] was performed with inclusion of temperature. After numerical calculations,
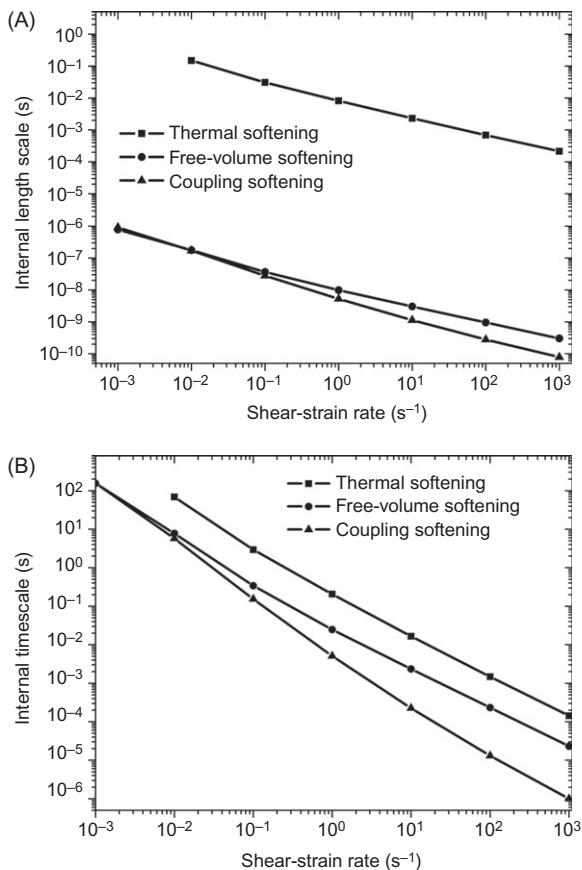
Figure 8.8 Stability analysis of the homogeneous deformation: the dependence of shear-strain rate on (A) the internal length scale and (B) the internal timescale.

they found that the catastrophic character of shear banding or strain localization is evident. Figure 8.9A illustrates the remarkable acceleration of strain development in the shear band after a peak stress has been reached and the corresponding drop of strain rate in the matrix. In addition, the great increase of strain rate in the band results in the rapid rise of the inner shear strain (Figure 8.9B), giving rise to a shear band. During such a process, the viscosity in the band drastically decreases to a value of approximately 10^{-5} poise, much smaller than that ($\sim 10^{11}$ poise) outside the band [20].

It is well known that the initiation of shear banding hinges strongly on the catastrophic drop of local viscosity. To ferret out the main reason for this material weakening, they calculated both the free-volume concentration and the temperature increase in the shear band during the shear deformation, as presented in Figure 8.10. Interestingly, it is noted that the sharp bend up in the curve of free-volume concentration is prior to that in the temperature rise. The result provides much clearer evidence that the local material softening or instability due to free-volume creation is earlier and faster than that due to temperature rise. This is consistent with that given by the
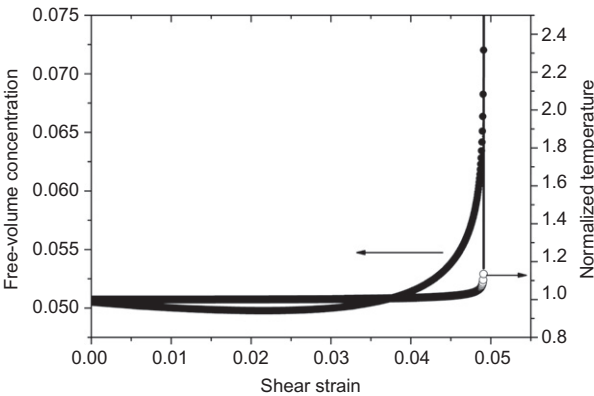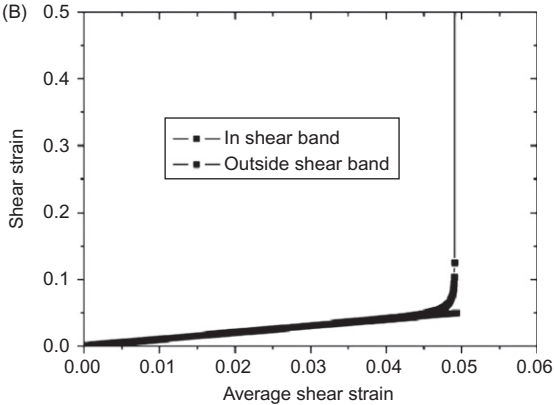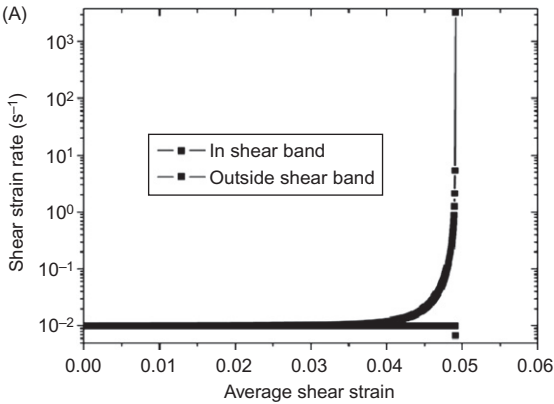
Figure 8.9 The shear-banding process. A history of (A) strain rate and (B) strain is shown for both the forming shear banding and the surrounding matrix.

Figure 8.10 The evolution of free-volume concentration and normalized temperature in the shear band as the applied shear strain increases.

linear perturbation analysis. In addition, the temperature rise is the consequence of free-volume-induced shear localization, not its cause; this agrees well with the deduction of many researchers based on experimental observations. In the next section, atomistic simulations also show that local heating occurs after the onset of localized

flow in amorphous alloys. In particular, these results provide a powerful theoretical expatiation on the puzzle about temperature rise at shear bands and thickness of shear bands in metallic glasses. The local free-volume creation, as the origin of shear localization, controls shear-band thickness (see Section 8.5 for more details), while local temperature rise, as a secondary effect, depends strongly on the development of this shear localization [128,129].

Both experiments and modelling show that large shear strain can be achieved in the shear band. Considering such large deformation, some finite-deformation coupled thermal−mechanical constitutive models of BMGs have been recently developed [126,127,132,133]. For example, the finite-deformation model proposed by Yang et al. [126] can well capture the quasi-static compression behaviour of Vit 1 BMG at RT. Further, they calculated the stress−strain curves with adiabatic heating at strain rates of 1.0×10^{-4}, 1 and $1.0 \times 10^{4} \, \mathrm{s}^{-1}$. In contrast to the isothermal case, a significant decrease of the stress, or strong strain softening, can be predicted. Thus they conclude that although the free-volume increase initiates the shear band, the subsequent temperature rise accelerates the localization of deformation. This result is satisfactorily consistent with the previous conclusion [20]. Very recently, Jiang et al. [134] performed a series of three-point bending experiments on as-cast and annealed samples of Vit 105 BMGs over a wide range of temperatures varying from RT to liquid nitrogen temperature (77 K). They found that the significant decrease of free volume within samples, corresponding to the decease of STZ volume, can result in the disappearance of shear banding. However, the shear banding can still occur even at 77 K. This confirms the dominated role of free volume on the shear-banding instability in BMGs.

8.4.3   Atomistic Modelling

The formation mechanism of a shear band presented previously captures many experimental observations in metallic glasses. However, current experimental techniques, including positron annihilation, ultrafast infrared imaging, TEM and SEM and AFM, have difficulties to study such shear localization processes that have extremely short timescales and very small length scales. Moreover, most tests have to be performed post-mortem after sample deformation or fracture. The conclusions drawn from these tests are, therefore, often partial and sometimes contradict each other. The molecular dynamics (MD) simulation is generally believed to be an effective way, providing an in situ and real-time observation of the shear localization at the atomic level. In particular, the characteristic sizes of shear bands in metallic glasses just fall into the reach of direct MD simulations. In the following, we present some recent works pertinent to the initiation of shear banding by using the MD method.

Physically, a shear band is a narrow region with the plastic shear strain larger than that in the rest of the sample. During MD simulations, we can record the position of each atom at each run-step and then identify the localized region undergoing larger shear deformation using the atomic positions recorded. Currently, there are three popular methods: 'stripe-painting', proposed by Bailey et al. [135]; $D_{\min}^{2}$, developed

by Falk and Langer [72] and the atomic local shear strain η_i^{Mises}, proposed by Shimizu et al. [136].

In the framework of an MD simulation, the Voronoi method is usually used to characterize the glass structure. If a shear band is developing in a sample, this method still has a capability of capturing the structural change. There are two ways to indicate the structural change during deformation. The first is to directly look at a specific type of coordinate polyhedron and its volume fraction in a sample [110]. The second way is to estimate the free volume based on the Voronoi volume v_{voro} of different types of polyhedral [109].

Very recently, Ma and co-workers [110] combined the two methods to monitor the local structural evolution in the early stage of shear banding. They performed the uni-axial compression on a Cu−Zr metallic glass, during which the shear band is indicated by η_i^{Mises}. Furthermore, they used the fraction of the Cu-centred full icosahedra (FI) as the key indicator of the glass structure. They observed that a band is developing, in which the FI motifs are lost preferentially relative to other regions in the sample. This decrease in the fraction of stable and shear-resistant FI causes structural softening. Such local structural softening corresponds to the generation of a Voronoi or free volume in the shear band. Similar results were obtained recently by Li and Li [108,109]; in addition, they analysed the distribution of the NN atomic bond lengths (ABLs) at various strains [108]. It was found that the ABLs increase with increasing strains in the shear-band region, while the ABLs outside remain small and uniform. These results indicate that the structural disordering or free volume in the shear band is much more significant than that outside. In other words, the initiation of the shear band is always accompanied by the local structural softening, which is consistent with the experimental observation [26,39,100] and the previous continuum mechanical analyses.

To check whether a shear band originates from the thermal softening or not, we must determine the temperature rise within the shear band. Ma and co-workers [110] investigated the evolution of the temperature rise in the sample during deformation. Note that in this initial stage of localization, the temperature rise in the band is less than 150 K; the band remains cold. Their results also show that the temperature rise lags behind the structural softening in the shear band. By investigating the D_{ave}^2 and temperature rise during localization, Bailey et al. [135] have obtained a similar result. The D_{ave}^2 localization occurs over the interval 5−10% strain, whereas the temperature rise is somewhat delayed; it does not start until just before 10% strain. The simulation results agree well with our shear-band analysis (see Figure 8.10); i.e. the temperature rise is not a cause of shear banding but a consequence. Based on small-scale MD simulations and thermo-mechanical analysis, Shimizu et al. [136,137] have proposed an aged-rejuvenation-glue-liquid (ARGL) model for an MSB, during which a critical length scale of the order for STZs to develop into an MSB is predicted. It is found that, at the later stage of shearing, the local temperature at the centre of the shear band has reached the glass transition temperature, which is consistent with the result of Yang et al. [119].

8.5 The Shear-Band Evolution Process

After it nucleates, a shear band would propagate forward driven by far-field loading. This post-instability process is inextricably linked to final fracture, which has attracted growing attention. In this section, we review recent advances in this area, notwithstanding that there is a great deal unknown about the phenomenon.

8.5.1 Shear-Band Propagation Dynamics

The first attempt to clarify the detailed process of shear banding in metallic glasses was performed by Masumoto and Murata in 1976 [138]. Using a very hard tensile machine, they indirectly inferred that shear-band propagation is rapid and intermittent. Shortly afterwards, Neuhäuser [139] made observations by high-speed cinematography on the development of shear bands during tension of $Pd_{80}Si_{20}$ ribbon and during bending of an Fe-based ribbon, and observed that the bands propagated across the sample in several rapid bursts with time intervals of several seconds between the bursts. However, due to the insufficient temporal resolution (up to 1.7 ms), the single burst of the shear band was not captured. Interestingly, he noted that a pre-existing shear band can slow down the growth of a neighbouring band. In addition, some bands have been observed to disappear totally or partially, similar to crack healing. By recording acoustic emission (AE) signals in tension-strained Zr-based BMGs, Vinogradov and Khonik [140] revealed that the microscopic features of the shear banding in BMGs are very nearly the same as those found for ribbon metallic glasses. The shear band propagates in a jump-like mode as reflected by numerous AE bursts. Based on the AE signal, the initiation of shear bands was probed by Klaumünzer et al. [141]. Recently, the infrared camera with 1000 Hz frames was used to observe in situ the dynamic shear-banding process in compression of Zr-based BMGs by Jiang et al. [68], considering that shear banding causes an increase in temperature. Such spatial resolution is still not able to seize a full shear-banding process. However, based on the successive video frames, they demonstrated the spatio-temporality of shear bands in metallic glasses, as illustrated schematically in Figure 8.11. With decreasing strain rates, the plastic flow tends to be inhomogeneous with time and homogeneous in space; while with increasing rates, the plastic flow tends to be homogeneous with time and inhomogeneous in space. The temporal feature of shear bands has been confirmed by Dai and coworkers [66,67]. They conducted MD nano-indentation of Cu−Zr metallic glasses at different loading rates. The simulation result showed that at higher strain rates, the shear-banding events operate successively, whereas at lower rates, the shear events occur intermittently, exhibiting inhomogeneity in time, as shown in Figure 8.12. In addition to the strain rate, the shear-band temperature can also affect its propagation behaviour. Cheng et al. [142] pointed out that if it can remain cold, a shear band can slide in a stick-slip manner. However, a hot shear band will directly develop into a runaway catastrophic failure.
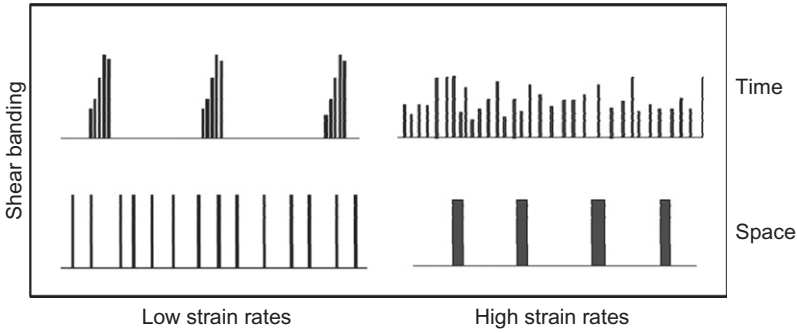
Figure 8.11 Schematic illustrations of temporal and spatial distributions of shear-banding operations at lower strain rates (left) and higher strain rates (right).
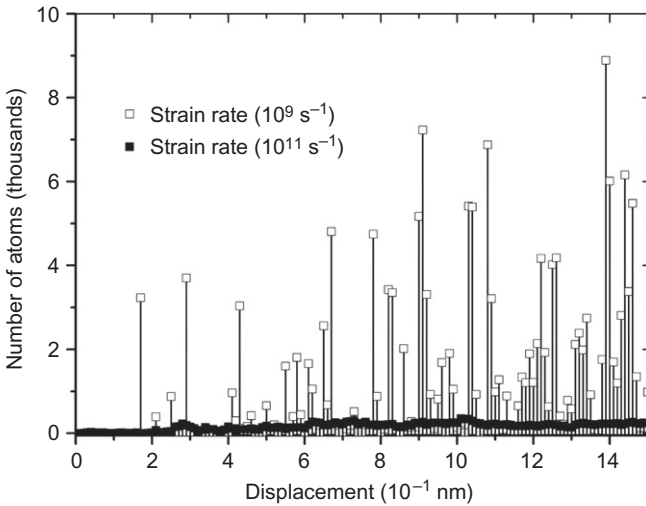

Figure 8.12 Temporal distributions of shear-banding events denoted by atoms with $D_{min}^2 > 0.15$ nm during nano-indentation at higher strain rates and lower strain rates.

Serrated plastic flow phenomena have been widely observed in BMGs under deformation-constrained loading modes such as compression [26,68,143−145] and indentation [63,95,146,147]. There is a general consensus that the shear banding in a sample should be responsible for the macroscopic flow serrations. Therefore, such serrations allow you to investigate shear-band dynamics. The flow serrations can appear as displacement bursts in the corresponding displacement−time curve. If you consider that such serrations or bursts are a result of intermittent operations of a main shear band, the velocity of the shear band can be calculated. However,

it must be pointed out that the velocity calculations should first be based on the assumption regarding the mode of shear-band propagation, i.e. simultaneous or progressive in fashion. For the first mode, the shear-band velocity has been calculated to be $10^1 - 10^3$ μm/s [143,145,148−150], which depends on the composition, ambient temperature, applied strain rate and sample size. Furthermore, the shear strain and viscosity within shear bands have been predicted [143,151]. For the second mode, the calculated velocity is about several metres per second at RT [149,152]. These velocities are many orders of magnitude smaller than one would expect, i.e. a shear-wave speed of approximately $10^2 - 10^3$ m/s. If we take approximately 10^0 m/s as the shear-band velocity and consider that such a shear band propagates across a millimetre-sized sample, the timescale of its propagation is the order of ms. However, the experimental techniques with a temporal resolution of approximately ms have not captured the propagation process of shear bands. The underestimation of shear-band velocity maybe from the premise of a *single* shear band. In fact, Vinogradov and Khonik [140] found that an individual serration corresponds to a bundle of AE signals; a signal corresponds to a shear band operating. It is therefore reasonable to believe that the serrations are due to the operation and interaction of multiple shear bands, rather than one main shear band, especially for the ductile BMGs. Very recently, Wang and co-workers [144] have revealed that the plastic flow serrations of ductile BMGs can evolve into a self-organized critical state characterized by the power-law distribution of shear avalanches. This implies that the intermittent motion of shear bands is scale free; i.e. there is not a dominant shear band. MD simulations show that the shear-band velocity can be close to the speed of sound at the early stage of shear banding when one shear band is propagating across the sample [110]. After it penetrates across the entire sample, the shear band slips simultaneously across the entire shear plane. The first simultaneous mode was captured by Song et al. [148] using a high-speed camera (up to 5000 Hz frame).

Very recently, by developing a dynamic 'forced' shear technique of hat-shaped specimens, the shear-band propagation mode was clearly determined by Jiang and Dai [30]. They observed the longitudinal section of a deformed Vit 1 hat-shaped specimen using high resolution scanning electron microscope and found that there is a crack stopper in the forced shear zone, as shown in Figure 8.13A. It can be seen from this picture that the crack with the well-defined tip does not penetrate through the shear zone. Further AFM observation exhibits that the crack is led by a shear band (see Figure 8.13B). Obviously, the shear band has a tip that nucleates at an inhomogeneous site. This provides solid evidence for the progressive propagation of shear bands in metallic glasses. In fact, similar phenomena have been widely observed in the literature [10,11,25,44,68,106,118,139]. If the crack could be arrested, the propagating shear band would finally penetrate the entire sample to reach the opposite surface. At that time, the shear band would operate in a simultaneous fashion; this is expected to occur in some ductile systems. Ma and co-workers [110] recently captured the transition of the shear-banding mode from progressive at small strains to a simultaneous fashion at very larger strains, using MD simulations. In reality, most BMGs display very limited ductility, especially in
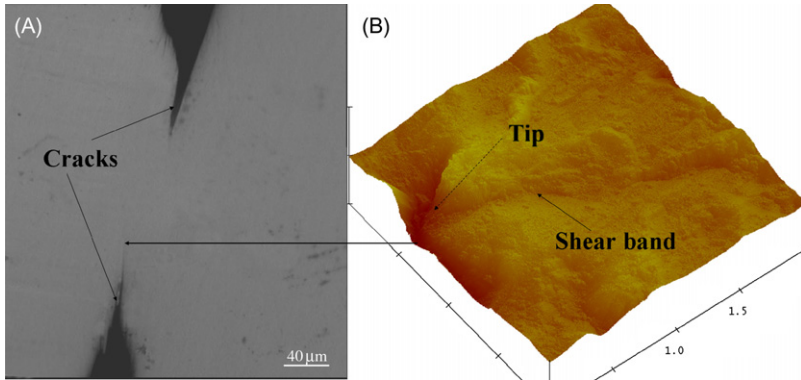
Figure 8.13 The shear zone in a deformed hat-shaped Vit 1 BMG specimen under dynamic forced shear, showing a stop crack that is led by a shear band with a well-defined tip.

tension or shearing. Therefore, the simultaneous propagation mode of a shear band occurs rarely in most cases.

8.5.2 Shear-Band Toughness

For an advancing shear band, a very basic question is how much energy the shear band can consume prior to catastrophic cracking. In other words, after the energy release Γ overcomes the critical plastic energy Γ_c, the shear band will mature to become a runaway shear crack. In this regard, the larger the Γ_c, the more significant is the toughness or ductility of BMGs. Γ_c therefore determines shear-band susceptibility that measures the intrinsic resistance of materials to the propagation of shear bands. Recent studies [153,154] have focused on the energy release Γ and further experimentally determined the Γ_c. Very recently, the shear-band toughness, initially proposed by Grady [155] for crystalline alloys, was extended to BMGs by Jiang and Dai [30]. They aim at theoretically describing the inherent susceptibility Γ_c to shear-band propagation in BMGs.

To characterize ASB susceptibility in crystalline alloys, Grady [155] introduced the concept of shear-band toughness, analogous to fracture toughness. As for BMGs, however, the shear banding exhibits some distinct features. When subjected to an external loading, some local regions, instead of the whole sample, preferentially yield via the cascade of a number of individual atomic jumps around free-volume sites [17] or STZs [18], forming local plastic regions (LPRs). The shear bands then nucleated simultaneously or successively in these LPRs. Finally, one of the nucleated shear bands dominates, propagates and causes a catastrophic fracture of the material. Furthermore, in addition to conventional energy/thermal and momentum/viscous dissipation, the free-volume dissipation should be involved in the shear-banding process in BMGs.

Based on the Grady−Kipp solution [155−157] and further considering shear-band stress softening due to both free-volume creation and temperature rise, the critical dissipation energy Γ_c can be analytically expressed (subscript '0' denotes the terms due to the sole free-volume softening) as [30]:

$$\left[1 - \Omega(\Gamma_c/\Gamma_{c0})^{1/3}(w/w_0) \right] \left[1 + \frac{(\Gamma_c/\Gamma_{c0})^{2/3}}{(w/w_0)^2} \right] = 2\frac{(\Gamma_c/\Gamma_{c0})}{(w/w_0)} \tag{8.4a}$$

with a dimensionless thermal-effect coefficient

$$\Omega = \left(\frac{2}{\alpha R} \right) \left(\frac{B}{Le} \right) \tag{8.4b}$$

where B accounts for the degree of thermal softening, α is the free-volume softening coefficient, the parameter R describes the local dilatation ability [158] and the Lewis number $Le = \chi/D$ measures the competition between thermal diffusivity and free-volume diffusivity. Equation (8.4) actually provides the implicit expression for Γ_c in a coupled free-volume softening and thermal-softening shear band. The concept of shear-band toughness is naturally introduced as [30]:

$$K_s = \sqrt{2G\Gamma_c} \tag{8.5}$$

which measures the internal resistance of BMG materials to propagation of shear bands. For the typical Vit 1 BMG, a shear-band toughness of $K_s \sim (2.66 - 26.58)$ MPa$\sqrt{m}$ is calculated, if considering the critical displacement ψ_c varies from 100 nm to 10 μm [118,121,128,153,159]. This calculated value range of K_s is expected to be smaller than the mode II fracture toughness ($K_{IIC} = 75$ MPa$\sqrt{m}$) of this material measured by Flores and Dauskardt [160]. It is expected that the shear-band toughness should contribute to the fracture toughness [161], and their relationship can be linked [30].

The functional dependence of the critical dissipation energy on the shear-band width under different thermal-effect coefficients, determined by Eq. (8.4), is shown in Figure 8.14. For comparison, the case without the thermal effect, i.e. $\Omega = 0$, corresponding to the bold line, was also calculated. From this graph, it is readily seen that all these curves have two branches − left and right − and each of them intersects at a local minimum. The physical mechanism is reasonably clear. For thinner bands (moving to the left branch), the enhanced free-volume diffusion restrains the rate of free-volume softening and leads to excessive dissipation [20,162]. Wider bands (moving to the right branch) are effectively free of free-volume diffusion. However, the accelerated diffusion of momentum (inertia) into the shear-band vicinity again limits the rate of free-volume softening and also incurs additional dissipation. The shear-band thicknesses near the local minimum properly balance
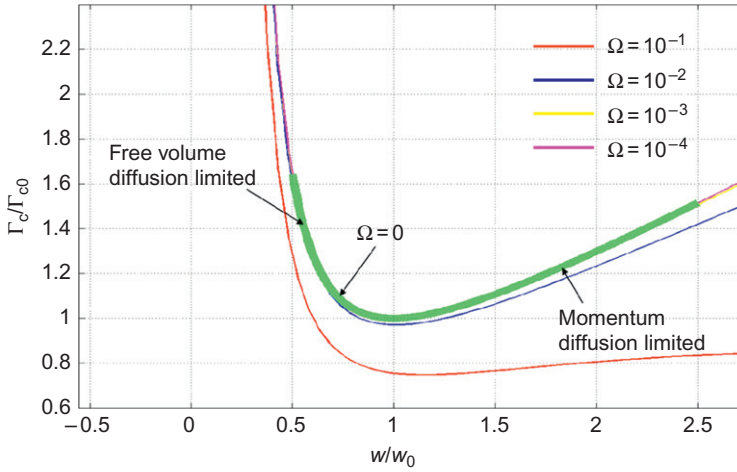
Figure 8.14 Plot of the critical energy dissipated in the shear band as a function of the shear-band thickness. All curves are provided by (8.4) in the text with different thermal-effect coefficients and are non-dimensionalized by the optimum shear-band thickness w_0 and the corresponding dissipation energy Γ_{c0} for the sole free-volume softening case.

the free-volume and momentum diffusion, providing the minimum possible shear-band dissipation. During the competition between the free-volume and momentum diffusion, the thermal softening, including its diffusion, plays a secondary role. As shown in Figure 8.14, with increasing the thermal-effect coefficient Ω from 10^{-4} to 10^{-1}, the optimum shear-band thickness increases slightly from w_0 to about $1.2w_0$; the corresponding optimum shear-band dissipation energy decreases somewhat from Γ_{c0} to $0.75\Gamma_{c0}$. This result clearly indicates that the thermal effect promotes the shear-band propagation because it decreases the critical energy barrier preventing the shear band from cracking. In particular, the insensitivity to thermal softening of the shear-band thickness indicates that the shear-band propagation in BMGs is governed by the free-volume softening.

8.5.3 Shear-Band Width

As we concluded earlier (Table 8.1), the characteristic width of shear bands is of the order of approximately 10 nm. Recently, finite STZ sizes of about $1-2$ nm (not reaching 2 nm) have been identified by much research [1,3,81,84,163]. Interestingly, the '10-times-rule' in granular materials [164] seems to be roughly satisfied in metallic glasses; i.e. the shear-band thicknesses are approximately 10 times the STZ sizes, implying a similar shear-instability mechanism between the two materials. However, the quantitative relationship between the thickness of the shear band and the STZ

size is still pending, and the precise underlying physics that dominates the shear-band width is not clear.

In crystalline alloys, the width of an ASB is supported by a balance of the plastic work-heat diffusion; its theoretical prediction has been successfully established by Dodd and Bai [165] and Walley [166]. In the same spirit, i.e. considering the free-volume coalescence-diffusion balance, Dai and Bai [19] derived an estimation of shear-band thickness in metallic glasses as:

$$w_0 \sim \sqrt{D \frac{\xi^*}{G^{\xi^*}}} \tag{8.6}$$

where * denotes the values within the band. Note that G^{ξ^*} is the net rate of free-volume increase and is highly dependent on the strain rate. You can reasonably assume that the thickness of an MSB is the final dimension of the perturbation with the initial wavelength, developed into the local steady-state flow in the post-instability stage. In this stage, the diffusion coefficient of the free-volume concentration is expected to obey the Stokes−Einstein equation [17,74]. Furthermore, based on the analogy between dislocation motion and the STZ operation, Eq. (8.6) can then yield [21]

$$w_0 = \frac{2\pi}{3} d \left(\xi^* \cdot \frac{1}{\gamma_c} \cdot \frac{1 + \nu}{1 - \nu} \right)^{1/2} \tag{8.7}$$

where d is roughly the STZ size, ξ^* is the activation free-volume concentration due to STZ-induced shear instability and γ_c is the average shear yield strain whose value is almost a universal constant of about 0.0267 for various systems [83]. This equation indicates that the correlation between the shear-band thickness and the STZ size does not follow a simple linear relation, and the influence of other parameters, such as ξ^*, γ_c and ν, should be involved. The dependence of these parameters on the shear-band width was examined. It is obvious that the shear-band thickness in metallic glasses is mainly governed by the STZ-activated free-volume concentration incurring instability and the STZ size.

Because the fundamental unit process underlying plastic flow is an STZ, the activation free volume facilitating local shear instability is actually the threshold of the free volume in activated STZs, beyond which the STZs become topologically unstable. At the atomic cluster level, the free-volume threshold must be a probability (usually Gaussian) distribution [17,18]. Egami's theory of topological fluctuations in the bonding network has predicted that if the average local transformation volume strain is larger than about 10%, the local atomic cluster site will become topologically unstable and be liquid like [167]. This average local volume strain can be analogous to the mathematical expectation of the probability distribution of a local STZ-activated free-volume concentration in plastic flow. In addition, the

recent work of Lu et al. [51] has also unveiled that the dividing line of free-volume concentration is about 0.10, between a densely packed structure with a coordination number (CN) of greater than 10 and a loose one with CN < 10. Therefore, we can reasonably choose $\xi^* \approx 0.10$, $d = 1.5$ nm and $\nu = 0.36$; the calculated shear-banding width is $w_0 \approx 9$ nm according to Eq. (8.7). This value agrees well with the characteristic thickness ($\sim$10 nm) of shear bands in various metallic glasses, demonstrating the intrinsic universality of local topological stability of STZs in glassy structures undergoing inhomogeneous plastic flow. The shear-band thickness is underpinned by a balance of the free-volume creation diffusion via the superposition of STZs. Thus, the local topological instability of STZs, together with their activation size and free volume, determines the width of the shear band in metallic glasses.

8.5.4 Shear-Band Spacing

During the process of loading, if one shear band is not sufficient to dissipate the applied energy, additional shear bands will form within samples. Certainly, such multiplication phenomenon of shear bands is sensitive to loading mode [26,56], sample geometry [168], material composition [169], atomic topological order [170] and so on. The operation of a single shear band will lead to stress unloading or strain relaxation in the vicinity of that shear band. Such local unloading or relaxation causes other shear bands to be excluded from that vicinity, resulting in multiple shear bands with characteristic spacing. In addition, the magnitude of shear-band extension can be represented by the shear displacement within the band. At the surface of the sample, the shear displacement behaves as a shear offset, which has been widely observed [120,121,171]. It is assumed that a critical shear displacement is required to create an MSB, and additional displacement may initiate fracture of the material along the band.

Bending is an effective method to investigate the shear-band patterns in metallic glasses [172]. Conner et al. [56,171] have carried out a series of experiments in which they bent beams made of Zr-based (Vit 106) metallic glasses of various thicknesses around mandrels of different radii. The nearly evenly spaced shear bands as well as the shear offsets at the free surfaces were observed. Furthermore, the sample thickness dependence of shear-band spacing and offset was quantitatively measured. Conner et al. [171] have performed an analysis of elastic perfectly plastic bending by treating the shear bands as mode II cracks. In their consideration, the maximum shear displacement occurs at the band end or the surface, while at the shear-band tip the displacement is zero. They derived expressions for the shear-band spacing and the shear offset, as well as their theoretical relationship. Later, Ravichandran and Molinari [173] performed a more precise analysis to capture the essential details of the shear-banding phenomena during bending. By balancing the dissipated energy as calculated from elasto-plastic beam theory and the energy dissipated along shear bands, and further introducing a failure criterion, they obtained an explicit form of shear-band spacing at failure. The shear-band offset was also derived. These predicted models for shear-band spacing offset capture the experimental observation taken from Conner et al. [56]. Based on the developed

finite-deformation constitutive model of plasticity of BMGs and by implementing the model in the finite-element programme, Yang et al. [126] simulated the bending experiment performed by Conner et al. [56]. Their simulation results show that the stress relaxation indeed happens due to the presence of a shear band, indicating a linear relationship between the zone size and the plate thickness. This agrees well with the experimental observation [56]. They further investigate the sample size dependence of shear-band spacing directly by allowing for the formation of multiple shear bands. The predicted almost linear spacing−thickness relationship is also in good agreement with both that predicted by the stress relaxation analysis and the experimental measurements of Conner et al. [56].

Recently, Zhang et al. [129] developed Grady's model and explained shear-band spacing in Zr-based BMGs under dynamic loads. They calculated the variation of shear-band spacing with strain rate, normal stress and critical shear displacement. It has been found that the shear-band spacing decreases with (a) increasing strain rate, (b) decreasing shear displacement and (c) decreasing normal stress. The results explained well their observed shear-band pattern beneath a dynamic Vickers indentation. Also note that the difference with and without the thermal effect is not significant for low confinement pressure and small shear displacement. They thought this is reasonable because they did not observe obvious heating phenomenon accompanying the shear bands even under such dynamic indentation. In the model of Zhang et al. [129], the shear displacement was considered to be constant along the shear band from its tip to its end. However, the experimental observation shows a different situation [118]. The shear displacement varies between almost zero and a maximum, with a value of zero at its tip, and the maximum (up to tens of micrometres) at its end. This variation can explain the scatter values of shear displacement that different researchers reported in different experiments [113,118,128,159,160].

It is noted that the question of when the shear band occurs in one dominated mode or in multiple mode has not been answered. What is the mechanism underlying the shear-band patterns in metallic glasses? To this end, Dai and co-workers [174] performed systematic four-point bending tests on Vit 1 BMGs. By developing a theoretical model that takes into account the structural feature of BMGs, they have revealed that the shear-band propagation is controlled by the free-volume softening, and, however, the resultant momentum diffusion results in the multiplication of shear bands with a certain characteristic spacing. The shear-band propagation and nucleation (multiplication) are controlled by their respective consumed energies. Recently, Jiang and Dai [97] performed a specific loading, i.e. turn machining, to investigate the multiple shear-band behaviour. It is found that the material removed exhibits a unique lamellar chip (Figure 8.15A) due to repeated shear-band formation in the primary shear zone (PSZ). Based on the experimental observations, a coupled thermo-mechanical orthogonal cutting model, taking into account force, free volume and energy balance in the PSZ, was developed, during which the lamellar chip formation or the periodic multiple shear bands can be understood as a self-sustained limit-cycle phenomenon (Figure 8.15B): there is autonomous feedback in stress, free volume and temperature in the PSZ. More specifically,
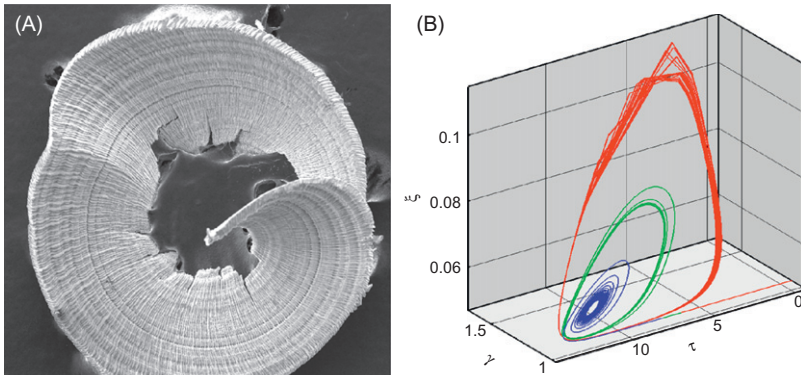
Figure 8.15 Lamellar chip morphology (A) of Vit 1 BMG and its underlying mechanism and (B) limit cycles.

such multiple shear bands occur as a result of the periodic loading−unloading cycle of material in the PSZ. It is revealed that the underlying mechanism is the symmetry breaking of free-volume flow and source, rather than thermal instability. The results, on the one hand, confirm the picture of how shear-band spacing results from stress relaxation [56,126,171,173]; on the other hand, it also provides clear experimental evidence for the physical origin of shear-banding instability in BMGs [20,27].

8.5.5 Pressure Sensitivity of Shear Banding

A lot of experimental observations [175−180] indicate that BMGs are pressure-sensitive materials. The pressure dependence of (localized) plastic deformation reflects the basic flow mechanism, which differs from that of their crystalline counterparts. Although the precise physical picture of how this dependence arises from the internal structure of BMGs remains elusive, it is plausible that it originates from atomic-scale dilatation [10,181,182]. Crystalline solids can deform at constant volume because the periodicity along slip planes provides identical atomic positions for sheared materials. However, a sheared portion of a BMG does not find such a perfect fit and thus will leave some holes. As we have known, the macroscopic flow of BMGs occurs by the cascade of STZs. As a result, STZs change into a loose configuration with a large volume, resulting in dilatation. Such dilatation induces hydrostatic stress during STZ formation, and thus the resultant macroscopic plastic flow should depend on pressure or normal stress.

Very recently, Dai and co-workers [183] derived an intrinsic theoretical correlation between the pressure-sensitivity coefficient and the dilatation factor in BMGs, taking shear-induced dilatation into consideration in STZ operations. The behaviour of STZs can be treated as an Eshelby-type inclusion problem [18]. To highlight the essential physics, let the initial spherical STZ experience a shape distortion and an

accompanied bulk dilatation. It is easy to deduce that the shear strain is 2β and volume strain is 3α during such an STZ operation. The relationship between shear-induced volume strain and shear strain is assumed to be linear, $3\alpha = \ell(2\beta)$, where ℓ is the dilatation factor measuring the ratio of dilatation to shear strain. Based on these considerations, the relationship between the pressure-sensitivity coefficient m and the dilatation factor ℓ is obtained, obeying

$$m = 3\ell/[30(1 - 2\nu)/(7 - 5\nu) + 2(1 + \nu)\ell^2/(1 - 2\nu)] \qquad (8.8)$$

Now one question naturally arises: How does shear-induced dilatation affect shear-banding instability in BMGs? To answer this question, Jiang and Dai [20] recently conducted the 1D simple shear analysis for pressure-sensitive BMGs. Figure 8.16 shows the internal length and timescales versus the dilatation factor with various pressure-sensitivity indices. Note that the internal scales for shear instability decrease with an increasing dilatation factor for any fixed m. This means
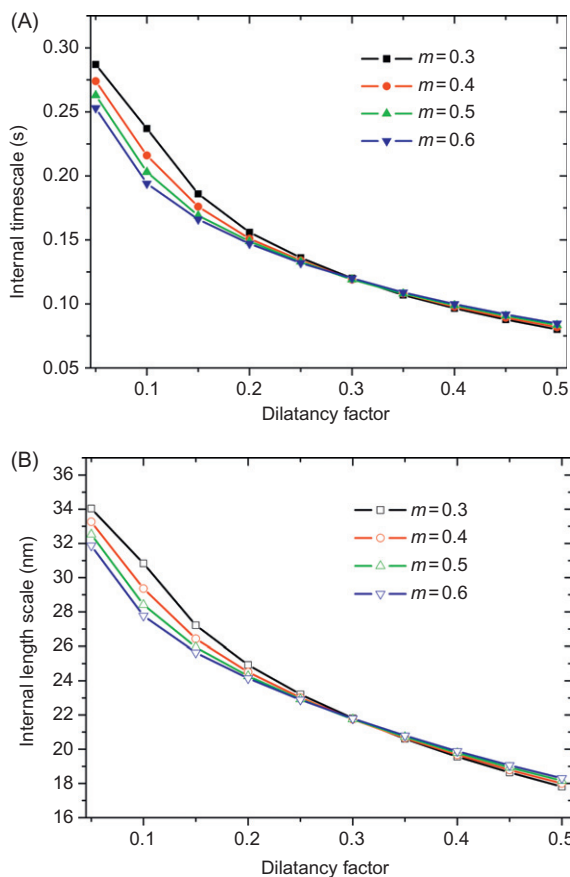

Figure 8.16 Internal (A) length scale and (B) timescale versus dilatation factor with various pressure-insensitivity indexes.

that the shear-induced dilatation strain makes the shear-banding instability easier and faster. In the fiducial interval (usually less than 0.3) of the dilatation factor, the tensile hydrostatic stress further aids shear instability according to the present results, which is consistent with the experimental observations by Flores and Dauskardt [178]. The present results show that the dilatation or the pressure sensitivity favours the origin or initiation of shear banding in metallic glasses.

The effect of pressure sensitivity on post-shear-banding behaviour has been investigated by Dubach et al. [176]. They found that with increasing pressure sensitivity, the intersection angle of two families of shear bands gradually departs from 90°. Moreover, Shi and Falk [184] have shown that the shear-band density significantly decreases with increasing pressure sensitivity, using MD simulations, in which they performed a series of uni-axial tensile tests on binary models of a glass with different degrees of structural relaxation. The enhanced pressure sensitivity or dilatation, on the one hand, facilitates the shear-banding initiation, and on the other hand, reduces the multiplication of shear bands. This is apparently paradoxical; however, it can be explained within the content of the free volume. It is well known that during structural relaxation, the free volume within samples is decreased. In such surroundings with a lower free-volume content, the STZ operations become more difficult because it requires more significant dilatation of the surrounding matrix. In fact, STZ operations occur preferentially in those regions having higher free volume as relatively less dilatation is required. Therefore, the relaxed samples with lower free-volume content hinder the formation of shear bands. However, for two samples with identical states (the same free-volume content), if one has more dilatation during deformation, i.e. creates more free volume, the shear-banding instability should initiate more easily in this sample.

8.6   Shear Bands and Global Ductility

Ductility is a mechanical property that describes the extent to which solid materials can be plastically deformed without fracture. Obviously, the ductility of BMGs is determined by the shear banding, which is the only mode for the RT plastic deformation. If the propagation of a dominant shear band can slow down or be in a stick-slip mode, then the onset of fracture might be delayed. In this case, the shear band is regarded to be 'cold' or stable [142]. In addition, multiplication of shear bands, i.e. distributing the plastic strain over many bands, contributes to global ductility [169,170,172]. Certainly, the most attractive way to improve the ductility is the suppression of shear bands, i.e. to achieve homogeneous deformation or necking prior to final fracture [185−187]. In this section, we discuss several approaches to this issue.

8.6.1   Loading Mode and Strain Rate

Under deformation-constrained loading conditions such as compression [26,68], rolling [188,189], bending [172] and indentation [190], obvious plastic flow can be

achieved. In those cases, the shear-band propagation is geometrically constrained. The emergence of plastic flow is of great interest for understanding the flow mechanism of this type of 'brittle' material [63,190]. However, those constrained geometries are too restrictive to be generally useful for load-bearing applications. After the geometrical restriction is released, the material still undergoes catastrophic failure with very limited ductility.

As discussed in Section 8.4.1, higher strain rates can promote shear-band formation in time. For some specific composites, if the resultant shear bands can distribute within samples as homogeneously as possible, it could enhance remarkably the global ductility not only in compression [191,192] but also in tension [192,193]. However, as pointed out by Jiang et al. [68], the shear banding preferentially operates in the same regions at a higher strain rate. So the BMG under higher strain rates stands a good change of forming a dominant shear band, which tends to lead to fast catastrophic fracture [22,25,194]. In addition, it is worth noting that dynamic strain rates ($>10^3\,\mathrm{s}^{-1}$) usually incur adiabatic heating, which also speeds up the transition of shear banding to unstable failure [20]. Therefore, although higher strain rates facilitate shear-band formation, the strain-rate dependence on ductility has a two-edged effect. The ductility is determined by the competition among the processes just mentioned: material and loading dependence.

8.6.2   Pre-treating

In conventional engineering materials, we can improve their mechanical properties by the pre-treating of samples such as introducing residual stress/strain (gradient) and severe plastic deformation. The similar pre-treating processes have also been applied to BMGs, in expectation of improving their ductility, even in tension. So far, there have been some pre-treating methods:

- Shot-peening [195]
- Pre-compression, including lateral [196], end-surface [197] and hydrostatic pressure [198]
- Surface wrap [199,200]
- Introducing a stress gradient [201]
- Releasing the boundary friction [202]
- Rolling [189].

Among them, shot-peening, pre-compression and rolling usually introduce residual stresses and/or inhomogeneous deformation, i.e. shear bands, into samples. For instance, Zhang et al. [195] carried out shot-peening of a Vit 1 BMG and found that the peened samples showed increased plasticity in bending and in compression. The enhanced ductility results from a combination of compressive residual stress, reducing the likelihood of surface cracking and more 'uniform' deformation induced by a high population of pre-existing shear bands. These pre-treatments, however, are not effective for improving the tensile ductility [189]. For the pre-compressive samples [196−198], their tensile ductility deserves further attention.

Surface wrap treatments actually allow the wrapped object, such as a Cu confinement sleeve [199] or Cu coating [200], to participate in the global deformation

that should be originally taken by the sample alone. In this case, even the already fractured sample induced by a dominant shear band still undergoes an applied stress. Therefore, the observed plasticity or ductility is actually *apparent*, which is similar to that arising from tilting or bending of specimens [201]. Very recently, Scudino et al. [202] investigated the effect of boundary conditions on the compressive plasticity of the Vit 1 BMGs by using a pure Cu foil as a lubricant material between loading platens and the sample. They found that the soft metal is very effective for reducing the contact friction at the platen−specimen interface, leading to a remarkable increase in plastic deformation with respect to the conventional semi-fluid MoS_2 lubricants or no lubricant. It seems that the more homogeneously the stress state is in the sample during deformation, the more ductile the deformation of the sample is. However, as mentioned earlier, the stress inhomogeneity/ gradient pre-existing in the sample favours plasticity [196,197,201]. The reason may be that the pre-existing stress gradient compensates for the stress inhomogeneity that arises during deformation. Also note that, in the present case, the Cu plates actually undertake a portion of deformation, which leads to a lower yield stress.

8.6.3 Sample Size and Machine Stiffness

In the early 1990s, Inoue et al. [203] observed that Fe-based and Co-based metallic glasses wires could exhibit good bending ductility only if the sample diameter was below a critical value. Such a size effect for ductility was studied quantitatively by Conner et al. [56,171], by bending Zr-based plates, ribbons and wires. They found that the strain to fracture increases markedly as the sample dimension decreases. Note that different sample sizes are produced in two ways. The first is samples with different sizes are cut from an identical as-cast plate or rod. Thus, the samples obtained are almost identical both chemically and structurally. In the second case, the samples with different sizes are directly cast from melt alloys and thus have distinct atomic structures due to different cooling rates. In this section, we only focus on the first case, i.e. the sole sample size effect. The structural factor will be discussed in the next section.

During MD simulations of uni-axial tension of Mg−Cu metallic glasses with scales of about 10 nm, Bailey et al. [135] have seen surprisingly that necking instability occurs before shear banding. They presumed that the disagreement with macroscopic observations comes from the local nature of a shear band compared with the 'global' nature of a necking instability. In a macroscopic sample, the effective 'wavelength' of the necking mode will be of the order of the sample size, while the characteristic size of a shear band is still of the order of tens of nanometres, which makes the latter much more likely to become unstable. Such a large difference in scale is lost in their simulations, in which the sample size is reduced to the shear-band size. Another factor that suppresses shear banding relative to necking is the necessity of breaking symmetry to choose the orientation of the shear plane. It is therefore expected that, in the rod sample down to 100 nm in diameter, necking instability is more likely to take place than the shear-banding instability. Recent experiments have confirmed this point. Actually, Jang and Greer [187] observed

the necking instability in the nano-tension of a specimen with a diameter of 100 nm. Similar necking phenomena have also been observed in the tension of metallic glass plates with dimensions of the order of 100 nm [186]. Most interestingly, during the tension of Al-based metallic glass with a size less than 20 nm, even an atomic chain was formed after sample necking [204]. In particular, homogeneous deformation can also be observed in compression [185,205], bending [185], even tension [206] of metallic glasses with similar characteristic sizes, during which the samples are usually constrained to some extent. Now it can be concluded that the critical nuclei size or approximately characteristic size of a shear band (usually tens of nanometres) separates the inhomogeneous from homogeneous deformation. If the sample size is larger than this value, then shear-banding instability occurs, and the sample exhibits brittle behaviour; in the other case, the necking instability or even homogeneous flow dominates, and the sample is ductile.

As mentioned in Section 8.5.1, Masumoto and Murata [138] have noticed the effect of machine stiffness on shear banding. They found that the higher the stiffness of the machine, the shear bands progressively become more stable. Recently, Han et al. [153] investigated quantitatively this effect considering a sample-machine system. Assuming the crack-like behaviour of a shear band, they derived an instability condition for shear-band propagation, given by:

$$S = \frac{\pi E d_s^2}{4 l_s \kappa_M} > S_{cr} \tag{8.9}$$

where κ_M is the stiffness of the testing machine, S_{cr} is a critical shear-band instability index that is a material parameter related to intrinsic plasticity and E, d_s and l_s are the Young's modulus, diameter and height of the sample, respectively. Equation (8.9) indicates that the larger the S (larger d_s and/or smaller κ_M for a fixed aspect ratio of the sample) the larger the possibility of shear-banding instability. Based on a series of compressive tests with a range of controlled values of sample size and machine stiffness, $S_{cr} \sim 0.72$ and ~ 4 are determined for the aspect ratios of 2 and 1, respectively. To modify the conflict with the sample-height effect on shear banding in Eq. (8.9), Cheng et al. [142] proposed a more precise factor for shear-banding instability $l_s (1 + S)$. Taking the energy balance of the shear-banding propagation into consideration in the sample-machine system, Yang et al. [154] arrived at a simple geometrical relation for the size-dependence ductility of BMGs:

$$L_{ext} = l_s + \iota d_s \geq L_{int} \tag{8.10}$$

where L_{ext} is an extrinsic length scale corresponding to the elastic energy release and ι is a dimensionless parameter accounting for the effect of machine stiffness; whereas L_{int} can be viewed as the internal resistance of a BMG to unstable shear banding and is independent of sample sizes. Unstable brittle fracture induced by the shear band will occur if $L_{ext} \geq L_{int}$. If the material is fixed, i.e. $L_{int} = $ constant,

L_{ext} should determine the shear-band behaviour and thus the ductility. Yang et al. [154] found that the ductility measured for the Zr-based BMGs with different simple geometries shows a very good correlation with the extrinsic length scale L_{ext}, here assuming $\iota = 1$ for simplicity. It predicts a critical intrinsic length scale of approximately 9 mm. It must be pointed out that the criteria just mentioned were obtained based on the compressive case. Extension of them to tensile cases needs to be attempted very carefully.

8.6.4   Composition and Atomic Configuration

The previous sections mainly discussed the effects of external factors on ductility of BMGs. Strictly speaking, the competition of external−internal factors determines the global ductility of metallic glasses, as indicated by Eq. (8.9) or (8.10). In this section, the intrinsic plasticity or ductility of materials is focused on. Poisson's ratio ν and equivalently the shear-bulk modulus ratio (G/K) criterion for intrinsic plasticity have been long established in crystalline alloys and are now found to be validated in metallic glasses. Lewandowski et al. [207] compiled a list of experimental data and found that there is a universal, sharp correlation for metallic glasses: they are intrinsically plastic for $G/K < 0.41 − 0.43$ or equivalently for $\nu > 0.31 − 0.32$. Recent research [169,208,209] has also demonstrated that the Poisson's ratio is a good indicator of the potential of metallic glasses to sustain plastic deformation. It is well known that elastic constants of a material are determined by its composition and microstructure. Therefore, a Poisson's ratio criterion allows us to understand the intrinsic plasticity of BMGs from the viewpoint of alloy composition and atomic configuration. For instance, through composition changes, Liu et al. [169] created some Zr-based BMGs that have relatively large ν values and display a capability to undergo multiple shear bandings and thus compressive ductility. Certainly, a specific soft−hard region structure (this will be discussed shortly) exists in their systems, which implies that the composition and structure are coupled to some degree in real cases.

When the alloy composition is fixed, different atomic configurations of BMGs can be obtained by changing the cooling history, i.e. the cooling rate. Shi and Falk [184] performed a series of uni-axial tests on binary models of metallic glasses by using MD simulations. It was revealed that the stress overshoot decreases as the cooling rate decreases. As we know, the stress overshoot is a measure of the tendency of shear banding. The larger the overshoot, the more metallic glasses are prone to shear localization. Recent experiments also show a similar tendency, although the sample size effect was included [168]. In the pure shear case, similar results have been obtained by Cheng et al. [210]. Furthermore, they examined the Poisson's ratio, configurational potential energy (CPE), shear modulus, bulk modulus and population of FI and fragmented polyhedral (FP) in the samples with different cooling rates. Table 8.2 includes these results for comparison. It can be found that the Poisson's ratio is higher in the sample with the higher cooling rate; its PEL is similar to that of a fragile liquid, with the higher CPE, the lower barrier of the megabasin and the lower effective curvature upon shearing at the basin bottom.

Table 8.2 Physical Properties of Metallic Glass Samples with High and Low Cooling Rates

Samples	High Cooling Rate	Low Cooling Rate
Stress overshoot	Low	High
Poisson's ratio	High	Low
PEL	(shallow curve)	(deep curve)
CPE	High	Low
Shear modulus	Low	High
Bulk modulus	Almost same	
Population of FI	Low	High
Population of FP	High	Low

The shear modulus G_c is then lower in this sample. With this PEL, the population of FI (solid-like clusters) is lower, whereas the concentration of FP (liquid-like clusters) is higher. A higher population of liquid-like clusters implies that there is a higher free-volume concentration within the sample. In this case, the shear localization occurs more easily or earlier, which is confirmed by Jiang and Dai [20]. In fact, the intrinsic correlation between fragility and Poisson's ratio in non-metallic glasses or metallic glasses has been reported by many researchers [211−214]. Because the bulk modulus corresponds to another dimension (hydrostatic expansion or shrinkage) in the PEL, which is correlated with valence electron density and not sensitive to configuration or cooling rates, when the composition is fixed, roughly, the lower the shear modulus of the sample, the more ductile the sample is. However, in the real case, the bulk modulus decreases with increasing cooling rate. Such a small decrease hardly affects the compressive ductility, but significantly degrades the tensile ductility, which will be discussed in detail in the following. According to the results of Cheng et al. [210], it can be concluded that the Poisson's ratio criterion for plasticity indeed has a structural origin [215].

In BMGs, the deformation mode is no longer anisotropic dislocation motion, which is sensitive to lattice types and slip planes, but rather an isotropic and universal one featured by the STZs. The STZ essentially is an SRO or MRO atomic cluster undergoing inelastic shear distortion. Assuming a Gaussian radial distribution function at SRO or MRO scale, Jiang and Dai [216] correlated the Poisson's ratio with the atomic structures of metallic glasses. The structural conditions for plasticity of BMGs can be concluded as follows:

- Atomic packing is denser.
- Such packing is more disordered.
- Atomic interaction is more anharmonic.

If the constituent atoms are fixed, i.e. the anharmonicity is identical, brittle BMG systems should have larger mean distances and less disorder. The opposite refers to plastic systems. However, the structural conditions for plasticity of BMGs,

i.e. higher atomic packing density and more significant atomic dispersion, are difficult to simultaneously satisfy during the real experimental process. A higher density of atomic packing can be achieved by structural relaxation or lowering the cooling rate during glass forming, during which atomic disorder is reduced. Hence a BMG becomes stiffer or harder. This is reflected in a change in the elastic constants and a decrease in the Poisson's ratio and embrittlement [207]. However, the disordered packing of atoms implies that a BMG is soft. Often, we can obtain a soft BMG with disordered atomic packing by using higher cooling rates, during which more randomly distributed free volume is inherited from the liquid. But such BMG systems have lower density of atomic packing, which is adverse to the plasticity, especially to the tensile ductility. It is expected that a monolithic BMG may be very plastic not only in compression but also in *tension*, when a *perfect* balance among the preceding conditions is realized by careful selection of its composition, controlling liquid−glass transition and temperature and/or mechanical treatments.

8.6.5   *Shear Banding in Metallic Glass Composites*

The pioneering work in this aspect was performed by Johnson and co-workers [217] aiming at defence applications. They fabricated Vit 1 matrix composites reinforced with uni-axially aligned tungsten wires and used them as kinetic energy penetrators, in which the BMG matrix shows self-sharpening behaviour due to localized shear-band failure, and the tungsten wires contribute to the kinetic energy due to high density. They found that the tungsten fibre-reinforced BMG composite has approximately a 10−20% improvement in penetrator efficiency over the tungsten heavy alloy. This research arouses growing interest due to its potential military value [218−221].

On the other hand, the concept of developing composites by combining the BMG matrix with second phases has been introduced to overcome the RT brittleness. Broadly, there are two types of BMG composites. One can be called 'in situ composites', where nanocrystalline phases or polymorphic glassy phases are growing in situ within the original metallic glass matrix [222−226]. The other is 'ex situ composites', where second-phase particles, fibres or slices are added to a melt prior to casting [221,227−232]. For whichever BMG composites, it is always anticipated that more shear bands, as well as deformation or transformation of second phases in some cases, contribute to macroscopic plastic strain before fracture, i.e. ductility. Therefore, the shear-banding behaviour in these composites and its interaction with second phases are of central significance.

Usually, the second phases have three contributions to ductility. Firstly, they create stress concentrations around their sides due to the mismatch resistance of them and glassy matrix to the external stress. Large numbers of shear bands can form from these stress-concentrated sites. To this end, 'soft' elastic/plastic inhomogeneities are often introduced into a glassy matrix [223,233−235]. Secondly, they act as the obstacle to shear-band propagation across the sample. After the shear bands encounter the second phases, these bands are either arrested or bypassed. To achieve this purpose, you should carefully choose the size and volume fraction of

the second phases. Matsumoto et al. [236] recently performed MD simulations of mode II deformation on a notched Zr-based BMG plate containing one nanocrystalline particle of Ni ahead of the notch base. They found that the resistance to shear banding is efficiently improved by introducing particles with sufficient size compared to the shear-band width. In addition, if you want to suppress the shear band in favour of cracking, Hofmann et al. [223] argue that the sizes of the second phases should match a material length scale related to fracture toughness, i.e. the size of a crack tip's 'plastic zone'. Schuh et al. [10] examined the effect of volume fraction of the second phase on the plastic strain to failure in compression and tension for a variety of composites. Data suggest that different second phases have different optimum volume fractions that are very sensitive to the matrix, loading mode and the respective sizes of the second phase and matrix. Thirdly, in some cases, the nanocrystalline second phase itself undergoes transformation, dislocation and twinning, which not only contributes to ductility but also produces work hardening [44,170,224,235].

Hays et al. [233] pioneered a quantitative analysis of the effects of second phase on the macroscopic plasticity. Based on the experimental observations, they concluded that the global plastic strain is controlled by the shear-band thickness and spacing. Obviously, overall plasticity or ductility can be improved by decreasing shear-band spacing by appropriately tailoring the microstructure. Very recently, Abdeljawad and Haataja [237] developed a diffuse-interface continuum model to examine the role plastic strain accumulates in ductile particles prior to shear banding. Based on a series of simulations, they suggested that the total plastic strain is a function of the particle size.

8.7   Prospects and Summary

As a unique deformation mode and a precursor of catastrophic failure, the nature of shear banding in metallic glasses has both scientific and practical significance. In this aspect, areas of interest involve (a) the geometrical configuration of shear bands such as thickness, length and spacing; (b) the structural change and temperature rise that occurs in shear bands; (c) the shear-band dynamics, including the propagating mode and velocity of shear bands; (d) the deformation accommodated by shear bands, including plastic strain and its strain rate; and (e) the shear-banding ductility relationship. Amongst them, the mechanism of shear-band formation and propagation is of central importance. In summary, we briefly provide some important conclusions:

- The shear-banding instability in metallic glasses initiates due to the coupled free-volume softening and thermal softening. Neither free-volume softening nor thermal softening can incur shear instability alone.
- During the shear-instability process, the free-volume softening plays the dominated role, whereas the thermal softening is a secondary effect. They contribute to each other. Physically, the shear band nucleates due to a cascade of stress-activated STZs or flow defects with the thermal fluctuation in the background.
- The shear-band evolution is a dissipation system, including thermal, momentum and free-volume dissipation from the shear band. The dissipated energy within the shear band is

determined by the balance between the momentum diffusion and the free-volume diffusion. The optimum dissipated energy corresponds to the shear-band thickness, about 10 nm. The momentum dissipation governs the shear-band spacing.

- The shear bands can branch, intersect, multiply, be arrested and even be suppressed, which contributes to the global plasticity of metallic glasses.

Nevertheless, there are many unresolved problems regarding shear bands in metallic glasses, which deserve further study. For example:

- *Shear-band dynamics*. The question of what modes the shear band propagates in has not been resolved well. The shear-band speed reported in the literature is confusing, from several micrometres to thousands of metres per second. How can an existing shear band disappear or stop? To answer these basic questions, it is urgent to develop proper experimental techniques with enough spatio-temporal resolution.
- *Shear-band-induced crack process*. A shear band finally evolves into a crack. It is not clear how a crack nucleates within a shear band. How to characterize the energy dissipation prior to cracking and crack nucleation needs to be studied.
- *Development of shear-band multiplication methodology*. So far, much work has focused on the compressive plasticity via the multiplication of shear bands. As for the deformation-unstrained loading case, e.g. uni-axial tension, these methods pose a great challenge. Developing shear-band multiplication methodologies suitable for the tension case is of more practical significance.
- *Shear banding in BMG derivatives*. The shear-banding process in pure BMGs has attracted much attention, in which its origin is reasonably clear, whereas the evolution process still remains unclear. However, the investigation of shear banding in BMG derivatives, including composites and porous materials, is still little understood. Current work is mainly confined to experimental observations and deals little with the quantitative description. Many questions deserve to be studied. For example, how does the introduction of a second phase (particle or void) affect the process of shear banding in the BMG matrix? If the ASB occurs in the second-phase particles, how do the two types of shear bands, i.e. the ASB and the free-volume-governed shear band, act together? How does the shear band within the matrix propagate through the second phases?

Acknowledgements

References

1. Miracle, D. B. (2004). A structural model for metallic glasses. *Nature Materials* **3**, 697−702.
2. Bernal, J. D. (1960). Geometry of the structure of monatomic liquids. *Nature* **185**, 68−70.

3. Sheng, H. W., Luo, W. K., Alamgir, F. M., Bai, J. M., and Ma, E. (2006). Atomic packing and short-to-medium range order in metallic glasses. *Nature* **439**, 419−425.

4. Egami, T. (2010). Understanding the properties and structure of metallic glasses at the atomic level. *Journal of the Minerals Metals and Materials Society* **62**, 70−75.

5. Hirata, A., Guan, P. F., Fujita, T., Hirotsu, Y., Inoue, A., Yavari, A. R., Sakurai, T., and Chen, M. W. (2011). Direct observation of local atomic order in a metallic glass. *Nature Materials* **10**, 28−33.

6. Greer, A. L. (1995). Metallic glasses. *Science* **267**, 1947−1953.

7. Johnson, W. L. (1999). Bulk glass-forming metallic alloys: Science and technology. *MRS Bulletin* **24**, 42−56.

8. Inoue, A. (2000). Stabilization of metallic supercooled liquid and bulk amorphous alloys. *Acta Materialia* **48**, 297−306.

9. Wang, W. H., Dong, C., and Shek, C. H. (2004). Bulk metallic glasses. *Materials Science and Engineering Reports* **44**, 45−89.

10. Schuh, C. A., Hufnagel, T. C., and Ramamurty, U. (2007). Mechanical behavior of amorphous alloys. *Acta Materialia* **55**, 4067−4109.

11. Trexler, M. M., and Thadhani, N. N. (2010). Mechanical properties of bulk metallic glasses. *Progress in Materials Science* **55**, 759−839.

12. Ashby, M. F., and Greer, A. L. (2006). Metallic glasses as structural materials. *Scripta Materialia* **54**, 321−326.

13. Schroers, J., Kumar, G., Hodges, T. M., Chan, S., and Kyriakides, T. R. (2009). Bulk metallic glasses for biomedical applications. *Journal of the Minerals Metals and Materials Society* **61**, 21−29.

14. Wang, W. H. (2009). Bulk metallic glasses with functional physical properties. *Advanced Materials* **21**, 4524−4544.

15. Inoue, A., and Takeuchi, A. (2011). Recent development and application products of bulk glassy alloys. *Acta Materialia* **59**, 2243−2267.

16. Huang, X., Ling, Z., Liu, Z. D., Zhang, H. S., and Dai, L. H. (2012). Amorphous alloy reinforced Whipple shield structure. *International Journal of Impact Engineering* **42**, 1−10.

17. Spaepen, F. (1977). A microscopic mechanism for steady state inhomogeneous flow in metallic glasses. *Acta Metallurgica* **25**, 407−415.

18. Argon, A. S. (1979). Plastic deformation in metallic glasses. *Acta Metallurgica* **27**, 47−58.

19. Dai, L. H., and Bai, Y. L. (2008). Basic mechanical behavior and mechanics of shear banding in BMGs. *International Journal of Impact Engineering* **35**, 704−716.

20. Jiang, M. Q., and Dai, L. H. (2009). On the origin of shear banding instability in metallic glasses. *Journal of the Mechanics and Physics of Solids* **57**, 1267−1292.

21. Jiang, M. Q., Wang, W. H., and Dai, L. H. (2009). Prediction of shear band thickness in metallic glass. *Scripta Materialia* **60**, 1004−1007.

22. Jiang, M. Q., Ling, Z., Meng, J. X., and Dai, L. H. (2008). Energy dissipation in fracture of bulk metallic glasses via inherent competition between local softening and quasi-cleavage. *Philosophical Magazine* **88**, 407−426.

23. Chen, Y., Jiang, M. Q., Wei, X. J., and Dai, L. H. (2011). Failure criterion for metallic glasses. *Philosophical Magazine* **91**, 4536−4554.

24. Huang, R., Suo, Z., Prevost, J. H., and Nix, W. D. (2002). Inhomogeneous deformation in metallic glasses. *Journal of the Mechanics and Physics of Solids* **50**, 1011−1027.

25. Liu, L. F., Dai, L. H., Bai, Y. L., Wei, B. C., and Eckert, J. (2005). Initiation and propagation of shear bands in Zr-based bulk metallic glass under quasi-static and dynamic shear loadings. *Journal of Non-Crystalline Solids* **351**, 3259−3270.

26. Liu, L. F., Dai, L. H., Bai, Y. L., Wei, B. C., and Eckert, J. (2005). Behavior of multiple shear bands in Zr-based bulk metallic glass. *Materials Chemistry and Physics* **93**, 174−177.

27. Dai, L. H., Yan, M., Liu, L. F., and Bai, Y. L. (2005). Adiabatic shear banding instability in bulk metallic glasses. *Applied Physics Letters* **87**, 141916.

28. Liu, L. F., Dai, L. H., Bai, Y. L., Wei, B. C., and Eckert, J. (2006). Characterization of rate-dependent shear behavior of Zr-based bulk metallic glass using shear-punch testing. *Journal of Materials Research* **21**, 153−160.

29. Gao, Y. F., Yang, B., and Nieh, T. G. (2007). Thermomechanical instability analysis of inhomogeneous deformation in amorphous alloys. *Acta Materialia* **55**, 2319−2327.

30. Jiang, M. Q., and Dai, L. H. (2011). Shear-band toughness of bulk metallic glasses. *Acta Materialia* **59**, 4525−4537.

31. Klement, W. I., Willens, R. H., and Duwez, P. (1960). Non-crystalline structure in solid-ified gold−silicon alloys. *Nature* **187**, 869−870.

32. Turnbull, D. (1950). Kinetics of heterogeneous nucleation. *Journal of Chemical Physics* **18**, 198−203.

33. Turnbull, D., and Cech, R. E. (1950). Microscopic observation of the solidification of small metal droplets. *Journal of Applied Physics* **21**, 804−810.

34. Chen, H. S., and Turnbull, D. (1969). Formation, stability and structure of palladium−silicon based alloy glasses. *Acta Metallurgica* **17**, 1021−1030.

35. Drehman, A. J., Greer, A. L., and Turnbull, D. (1982). Bulk formation of a metallic glass: Pd40Ni40P20. *Applied Physics Letters* **41**, 716−717.

36. Inoue, A., Zhang, T., Nishiyama, N., Ohba, K., and Masumoto, T. (1993). Preparation of 16 mm diameter rod of amorphous Zr65Al7.5Ni10Cu17.5 alloy. *Materials Transactions, JIM* **34**, 1234−1237.

37. Peker, A., and Johnson, W. L. (1993). A highly processable metallic glass: Zr41.2Ti13.8Cu12.5Ni10.0Be22.5. *Applied Physics Letters* **63**, 2342−2344.

38. Inoue, A., Zhang, T., and Masumoto, T. (1989). Al−La−Ni amorphous alloys with a wide supercooled liquid region. *Materials Transactions, JIM* **30**, 965−972.

39. Pampillo, C. A. (1975). Flow and fracture in amorphous alloys. *Journal of Materials Science* **10**, 1194−1227.

40. Chen, H. S. (1974). Thermodynamic considerations on the formation and stability of metallic glasses. *Acta Metallurgica* **22**, 1505−1511.

41. Inoue, A., Zhang, T., and Masumoto, T. (1990). Zr−Al−Ni amorphous alloys with high glass transition temperature and significant supercooled liquid region. *Materials Transactions, JIM* **31**, 177−183.

42. Löffler, J. F. (2003). Bulk metallic glasses. *Intermetallics* **11**, 529−540.

43. Greer, A. L., and Ma, E. (2007). Bulk metallic glasses: At the cutting edge of metals research. *MRS Bulletin* **32**, 611−615.

44. Chen, M. W. (2008). Mechanical behavior of metallic glasses: Microscopic understanding of strength and ductility. *Annual Review of Materials Research* **38**, 445−469.

45. Schroers, J. (2009). Processing of bulk metallic glass. *Advanced Materials* **21**, 1−32.

46. Gene Ice, (2005). Characterizing amorphous strain. *Nature Materials* **4**, 17−18.

47. Bernal, J. D., and Mason, J. (1960). Co-ordination of randomly packed spheres. *Nature* **188**, 910−911.

48. Dong, C., Wang, Q., Qiang, J. B., Wang, Y. M., Jiang, N., Han, G., Li, Y. H., Wu, J., and Xia, J. H. (2007). From clusters to phase diagrams: Composition rules of quasicrystals and bulk metallic glasses. *Journal of Physics D: Applied Physics* **40**, R273−R291.

49. Ma, D., Stoica, A. D., and Wang, X.-L. (2009). Power-law scaling and fractal nature of medium-range order in metallic glasses. *Nature Materials* **8**, 30−34.
50. Cheng, Y. Q., and Ma, E. (2011). Atomic-level structure and structure−property relationship in metallic glasses. *Progress in Materials Science* **56**, 379−473.
51. Liu, X. J., Chen, C. L., Hui, X., Liu, T., and Lu, Z. P. (2008). Ordered clusters and free volume in a Zr−Ni metallic glass. *Applied Physics Letters* **93**, 011911.
52. Inoue, A., and Nishiyama, N. (2007). New bulk metallic glasses for applications as magnetic-sensing, chemical, and structural materials. *MRS Bulletin* **32**, 651−658.
53. Luborsky, F. E., Frischmann, P. G., and Johnson, L. A. (1980). Amorphous materials − a new class of soft magnetic alloys. *Journal of Magnetism and Magnetic Materials* **19**, 130−137.
54. Tang, M. B., Bai, H. Y., Pan, M. X., Zhao, D. Q., and Wang, W. H. (2005). Bulk metallic superconductive La60Cu20Ni10Al10 glass. *Journal of Non-Crystalline Solids* **351**, 2572−2575.
55. Eliaz, N., Fuks, D., and Eliezer, D. (1999). A new model for the diffusion behavior of hydrogen in metallic glasses. *Acta Materialia* **47**, 2981−2989.
56. Conner, R. D., Li, Y., Nix, W. D., and Johnson, W. L. (2004). Shear band spacing under bending of Zr-based metallic glass plates. *Acta Materialia* **52**, 2429−2434.
57. Grimberg, A., Baur, H., Bochsler, P., Bühler, F., Burnett, D. S., Hays, C. C., Heber, V. S., Jurewicz, A. J. G, and Wieler, R. (2006). Solar wind neon from genesis: Implications for the lunar noble gas record. *Science* **314**, 1133−1135.
58. Liu, L., Qiu, C. L., Huang, C. Y., Yu, Y., Huang, H., and Zhang, S. M. (2009). Biocompatibility of Ni-free Zr-based bulk metallic glasses. *Intermetallics* **17**, 235−240.
59. Inoue, A., and Takeuchi, A. (2010). Recent development and applications of bulk glassy alloys. *International Journal of Applied Glass Science* **1**, 273−295.
60. Taub, A. I., and Spaepen, F. (1980). The kinetics of structural relaxation of a metallic glass. *Acta Metallurgica* **28**, 1781−1788.
61. Taub, A. I. (1980). Stree-strain rate dependent of homogeneous flow in metallic glasses. *Acta Metallurgica* **28**, 633−637.
62. Wang, D., Liao, G., Pan, J., Tang, Z., Peng, P., Liu, L., and Shi, T. (2009). Superplastic micro-forming of Zr65Cu17.5Ni10Al7.5 bulk metallic glass with silicon mold using hot embossing technology. *Journal of Alloys and Compounds* **484**, 118−122.
63. Schuh, C. A., Lund, A. C., and Nieh, T. G. (2004). New regime of homogeneous flow in the deformation map of metallic glasses: Elevated temperature nanoindentation experiments and mechanistic modeling. *Acta Materialia* **52**, 5879−5891.
64. Shi, Y. F., and Falk, M. L. (2007). Stress-induced structural transformation and shear banding during simulated nanoindentation of a metallic glass. *Acta Materialia* **55**, 4317−4324.
65. Subhash, G., and Zhang, H. W. (2007). Dynamic indentation response of ZrHf-based bulk metallic glasses. *Journal of Materials Research* **22**, 478−485.
66. Jiang, S. Y., Jiang, M. Q., Dai, L. H., and Yao, Y. G. (2008). Atomistic origin of rate-dependent serrated plastic flow in metallic glasses. *Nanoscale Research Letters* **3**, 524−529.
67. Jiang, M. Q., Jiang, S. Y., Ling, Z., and Dai, L. H. (2009). Smaller Deborah number inducing more serrated plastic flow of metallic glass. *Computational Materials Science* **46**, 767−771.
68. Jiang, W. H., Fan, G. J., Liu, F. X., Wang, G. Y., Choo, H., and Liaw, P. K. (2008). Spatiotemporally inhomogeneous plastic flow of a bulk-metallic glass. *International Journal of Plasticity* **24**, 1−16.

69. Lee, S. C., Lee, C. M., Lee, J. C., Kim, H. J., Shibutani, Y., Fleury, E., and Falk, M. L. (2008). Structural disordering process of an amorphous alloy driven by the elastostatic compression at room temperature. *Applied Physics Letters* **92**, 151906.

70. Park, K. W., Lee, C. M., Lee, M. R., Fleury, E., Falk, M. L., and Lee, J. C. (2009). Paradoxical phenomena between the homogeneous and inhomogeneous deformations of metallic glasses. *Applied Physics Letters* **94**, 021907.

71. Furukawa, A., and Tanaka, H. (2009). Inhomogeneous flow and fracture of glassy materials. *Nature Materials* **8**, 601−609.

72. Falk, M. L., and Langer, J. S. (1998). Dynamics of viscoplastic deformation in amorphous solids. *Physical Review E* **57**, 7192−7205.

73. Heggen, M., Spaepen, F., and Feuerbacher, M. (2005). Creation and annihilation of free volume during homogeneous flow of a metallic glass. *Journal of Applied Physics* **97**, 033506.

74. Cohen, M. H., and Turnbull, D. (1959). Molecular transport in liquids and glasses. *Journal of Chemical Physics* **31**, 1164−1169.

75. Turnbull, D. (1961). Free-volume model of the amorphous phase: Glass transition. *Journal of Chemical Physics* **34**, 120−125.

76. Polk, D. E., and Turnbull, D. (1972). Flow of melt and glass forms of metallic alloys. *Acta Metallurgica* **20**, 493−498.

77. Argon, A. S., and Kuo, H. Y. (1979). Plastic flow in a disordered bubble raft (an analog of a metallic glass). *Materials Science and Engineering* **39**, 101−109.

78. Eshelby, J. D. (1957). The determination of the elastic field of an ellipsoidal inclusion, and related problems. *Proceedings of the Royal Society of London Series A* **241**, 376−396.

79. Eshelby, J. D. (1959). The elastic field outside an ellipsoidal inclusion. *Proceedings of the Royal Society of London Series A* **252**, 561−569.

80. Spaepen, F. (1981). Defects in amorphous metals. In "*Physics of defects*" (R. Balian, M. Kleman, and J. Poirier, Eds.), North-Holland: Amsterdam, pp. 146−162.

81. Pan, D., Inoue, A., Sakurai, T., and Chen, M. W. (2008). Experimental characterization of shear transformation zones for plastic flow of bulk metallic glasses. *Proceedings of the National Academy of Sciences* **105**, 14769−14772.

82. Schall, P., Weitz, D. A., and Spaepen, F. (2007). Structural rearrangements that govern flow in colloidal glasses. *Science* **318**, 1895−1899.

83. Johnson, W. L., and Samwer, K. (2005). A universal criterion for plastic yielding of metallic glasses with a $(T/T_\mathrm{g})^{2/3}$ temperature dependence. *Physical Review Letters* **95**, 195501.

84. Mayr, S. G. (2006). Activation energy of shear transformation zones: A key for understanding rheology of glasses and liquids. *Physical Review Letters* **97**, 195501.

85. Harmon, J. S., Demetriou, M. D., Johnson, W. L., and Samwer, K. (2007). Anelastic to plastic transition in metallic glass-forming liquids. *Physical Review Letters* **99**, 135502.

86. Stillinger, F. H., and Weber, T. A. (1984). Packing structures and transitions in liquids and solids. *Science* **225**, 983−989.

87. Stillinger, F. H. (1995). A topographic view of supercooled liquids and glass formation. *Science* **267**, 1935−1939.

88. Debenedetti, P. G., and Stillinger, P. H. (2001). Supercooled liquids and the glass transition. *Nature* **410**, 259−267.

89. Frenkel, J. (1926). The theory of the elastic limit and the solidity of crystal bodies. *Zeitschrift fur Physik* **37**, 572−609.

90. Yu, H. B., Wang, W. H., Bai, H. Y., Wu, Y., and Chen, M. W. (2010). Relating activation of shear transformation zones to relaxations in metallic glasses. *Physical Review B* **81**, 220201(R).

91. Steif, P. S., Spaepen, F., and Hutchinson, J. W. (1982). Strain localization in amorphous metals. *Acta Metallurgica* **30**, 447−455.

92. Vaks, V. G. (1991). Possible mechanism for formation of localized shear bands in amorphous alloys. *Physics Letters A* **159**, 174−178.

93. Wright, W. J., Hufnagel, T. C., and Nix, W. D. (2003). Free volumn coalescence and void formation in shear bands in metallic glass. *Journal of Applied Physics* **93**, 1432−1437.

94. Leamy, H. J., Chen, H. S., and Wang, T. T. (1972). Plastic flow and fracture of metallic glass. *Metallurgical Transactions* **3**, 699−708.

95. Dai, L. H., Liu, L. F., Yan, M., Wei, B. C., and Eckert, J. (2004). Serrated plastic flow in a Zr-based bulk metallic glass during nanoindentation. *Chinese Physics Letters* **21**, 1593−1595.

96. Liu, L. F., Dai, L. H., Bai, Y. L., Wei, B. C., and Yu, G. S. (2005). Strain rate-dependent compressive deformation behavior of Nd-based bulk metallic glass. *Intermetallics* **13**, 827−832.

97. Jiang, M. Q., and Dai, L. H. (2009). Formation mechanism of lamellar chip in machining bulk metallic glass. *Acta Materialia* **57**, 2730−2738.

98. Mukaia, T., Nieh, T. G., Kawamura, Y., Inoue, A., and Higashi, K. (2002). Dynamic response of a Pd40Ni40P20 bulk metallic glass in tension. *Scripta Materialia* **46**, 43−47.

99. Masumoto, T., and Maddin, R. (1971). The mechanical properties of palladium 20 a/o silicon alloy quenched from the liquid state. *Acta Metallurgica* **19**, 725−741.

100. Donovan, P., and Stobbs, W. M. (1981). The structure of shear bands in metallic glasses. *Acta Metallurgica* **29**, 1419−1436.

101. Pekarskaya, E., Kim, C. P., and Johnson, W. L. (2001). In situ transmission electron microscopy studies of shear bands in a bulk metallic glass based composite. *Journal of Materials Research* **16**, 2513−2518.

102. Li, J., Spaepen, F., and Hufnagel, T. C. (2002). Nanometre-scale defects in shear bands in a metallic glass. *Philosophical Magazine* **82**, 2623−2630.

103. Jiang, W. H., and Atzmon, M. (2006). Mechanically-assisted nanocrystallization and defects in amorphous alloys: A high-resolution transmission electron microscopy study. *Scripta Materialia* **54**, 333−336.

104. Gu, X., Livi, K. J. T., and Hufnagel, T. C. (2003). Structure of shear bands in zirconium-based metallic glasses observed by transmission electron microscopy. Materials Research Society Symposium Proceedings **754**, CC7.9.1−CC7.9.6.

105. Chen, M. W., Inoue, A., Zhang, W., and Sakurai, T. (2006). Extraordinary plasticity of ductile bulk metallic glasses. *Physical Review Letters* **96**, 245502.

106. Kim, K. B., Das, J., Lee, M. H., Li, S., Fleury, E., Zhang, Z. F., Wang, W. H., and Eckert, J. (2008). Propagation of shear bands in a CuZrAl bulk metallic glass. *Journal of Materials Research* **23**, 6−12.

107. Pampillo, C. A. (1972). Localized shear deformation in a glassy metal. *Scripta Metallurgica* **6**, 915−918.

108. Li, Q. K., and Li, M. (2006). Atomic scale characterization of shear bands in an amorphous metal. *Applied Physics Letters* **88**, 241903.

109. Li, Q. K., and Li, M. (2007). Atomistic simulations of correlations between volumetric change and shear softening in amorphous metals. *Physical Review B* **75**, 094101.

110. Cao, A. J., Cheng, Y. Q., and Ma, E. (2009). Structural processes that initiate shear localization in metallic glass. *Acta Materialia* **57**, 5146−5155.

111. Flores, K. M., Sherer, E., Bharathula, A., Chen, H., and Jean, Y. C. (2007). Sub-nanometer open volume regions in a bulk metallic glass investigated by positron annihilation. *Acta Materialia* **55**, 3403−3411.

112. Liu, C. T., Heatherly, L., Easton, D. S., Carmichael, C. A., Schneibel, J. H., Chen, C. H., Wright, J. L., Yoo, M. H., Horton, J. A., and Inoue, A. (1998). Test environments and mechanical properties of Zr-base bulk amorphous alloys. *Metallurgical and Materials Transactions A* **29A**, 1811−1820.

113. Wright, W. J., Schwarz, R. B., and Nix, W. D. (2001). Localized heating during serrated plastic flow in bulk metallic glasses. *Materials Science and Engineering A* **319−321**, 229−232.

114. Hufnagel, T. C., Jiao, T., Li, Y., Xing, L.-Q., and Ramesh, K. T. (2002). Deformation and failure of Zr57Ti5Cu20Ni8Al10 bulk metallic glass under quasi-static and dynamic compression. *Journal of Materials Research* **17**, 1441−1445.

115. Lewandowski, J. J., and Greer, A. L. (2006). Temperature rise at shear bands in metallic glasses. *Nature Materials* **5**, 15−18.

116. Miracle, D. B., Concustell, A., Zhang, Y., Yavari, A. R., and Greer, A. L. (2011). Shear bands in metallic glasses: Size effects on thermal profiles. *Acta Materialia* **59**, 2831−2840.

117. Bruck, H. A., Rosakis, A. J., and Johnson, W. L. (1996). The dynamic compressive behavior of beryllium bearing bulk metallic glasses. *Journal of Materials Research* **11**, 503−511.

118. Yang, B., Morrison, M. L., Liaw, P. K., Buchanan, R. A., and Wang, G. (2005). Dynamic evolution of nanoscale shear bands in a bulk-metallic glass. *Applied Physics Letters* **86**, 141904.

119. Yang, B., Liu, C. T., Nieh, T. G., Morrison, M. L., Liaw, P. K., and Buchanan, R. A. (2006). Localized heating and fracture criterion in bulk metallic glasses. *Journal of Materials Research* **21**, 915−922.

120. Georgarakis, K., Aljerf, M., Li, Y., LeMoulec, A., Charlot, F., Yavari, A. R., Chornokhvostenko, K., Tabachnikova, E., Evangelakis, G. A., Miracle, D. B., Greer, A. L., and Zhang, T. (2008). Shear band melting and serrated flow in metallic glasses. *Applied Physics Letters* **93**, 031907.

121. Guo, H., Wen, J., Xiao, N. M., Zhang, Z. F., and Sui, M. L. (2008). The more shearing, the thicker shear band and heat-affected zone in bulk metallic glass. *Journal of Materials Research* **23**, 2133−2138.

122. Zhang, Y., Stelmashenko, N. A., Barber, Z. H., Wang, W. H., Lewandowski, J. J., and Greer, A. L. (2007). Local temperature rises during mechanical testing of metallic glasses. *Journal of Materials Research* **22**, 419−427.

123. Spaepen, F. (2006). Must shear bands be hot? *Nature Materials* **5**, 7−8.

124. Steif, P. S., Spaepen, F., and Hutchinson, J. W. (1983). Ductile versus brittle behavior of amorphous metals. *Journal of the Mechanics and Physics of Solids* **31**, 359−388.

125. Gao, Y. F. (2006). An implicit finite element method for simulating inhomogeneous deformation and shear bands of amorphous alloys based on the free-volume model. *Modelling and Simulation in Materials Science and Engineering* **14**, 1329.

126. Yang, Q., Mota, A., and Ortiz, M. (2006). A finite-deformation constitutive model of bulk metallic glass plasticity. *Computational Mechanics* **37**, 194−204.

127. Thamburaja, P., and Ekambaram, R. (2007). Coupled thermo-mechanical modelling of bulk-metallic glasses: Theory, finite-element simulations and experimental verification. *Journal of the Mechanics and Physics of Solids* **57**, 1263−1273.

128. Zhang, H. W., Subhash, G., and Maiti, S. (2007). Local heating and viscosity drop during shear band evolution in bulk metallic glasses under quasistatic loading. *Journal of Applied Physics* **102**, 043519.

129. Zhang, H. W., Maiti, S., and Subhash, G. (2008). Evolution of shear bands in bulk metallic glasses under dynamic loading. *Journal of the Mechanics and Physics of Solids* **56**, 2171−2187.

130. Yang, Y., Ye, J. C., Lu, J., Gao, Y. F., and Liaw, P. K. (2010). Metallic glasses: Gaining plasticity for microsystems. *Journal of the Minerals Metals and Materials Society* **62**, 93−98.

131. Bai, Y. L. (1982). Thermo-plastic instability in simple shear. *Journal of the Mechanics and Physics of Solids* **30**, 195−207.

132. Anand, L., and Su, C. (2005). A theory for amorphous viscoplastic materials undergoing finite deformations, with application to metallic glasses. *Journal of the Mechanics and Physics of Solids* **53**, 1362−1396.

133. Thamburaja, P. (2011). Length scale effects on the shear localization process in metallic glasses: A theoretical and computational study. *Journal of the Mechanics and Physics of Solids* **59**, 1552−1575.

134. Jiang, F., Jiang, M. Q., Wang, H. F., Zhao, Y. L., He, L., and Sun, J. (2011). Shear transformation zone volume determining ductile−brittle transition of bulk metallic glasses. *Acta Materialia* **59**, 2057−2068.

135. Bailey, N. P., Schiøtz, J., and Jacobsen, K. W. (2006). Atomistic simulation study of the shear band deformation mechanism in Mg−Cu metallic glasses. *Physical Review B* **73**, 064108.

136. Shimizu, F., Ogata, S., and Li, J. (2007). Theory of shear banding in metallic glasses and molecular dynamics calculations. *Materials Transactions* **48**, 2923−2927.

137. Shimizu, F., Ogata, S., and Li, J. (2006). Yield point of metallic glass. *Acta Materialia* **54**, 4293−4298.

138. Masumoto, T., and Murata, T. (1976). Deformation of amorphous metals. *Materials Science and Engineering* **25**, 71−75.

139. Neuhäuser, H. (1978). Rate of shear band formation in metallic glasses. *Scripta Metallurgica* **12**, 471−474.

140. Vinogradov, A. Y., and Khonik, V. A. (2004). Kinetics of shear banding in a bulk metallic glass monitored by acoustic emission measurements. *Philosophical Magazine* **84**, 2147−2166.

141. Klaumünzer, D., Lazarev, A., Maaß, R., Dalla Torre, F. H., Vinogradov, A., and Löffler, J. F. (2011). Probing shear-band initiation in metallic glasses. *Physical Review Letters* **107**, 185502.

142. Cheng, Y. Q., Han, Z., Li, Y., and Ma, E. (2009). Cold versus hot shear banding in bulk metallic glass. *Phyical Review B* **80**, 134115.

143. Song, S. X., and Nieh, T. G. (2009). Flow serration and shear band viscosity during inhomogeneous deformation of a Zr-based bulk metallic glass. *Intermetallics* **17**, 762−767.

144. Sun, B. A., Yu, H. B., Jiao, W., Bai, H. Y., Zhao, D. Q., and Wang, W. H. (2010). Plasticity of ductile metallic glasses: A self-organized sritical state. *Physical Review Letters* **105**, 035501.

145. Maaβ, R., Klaumünzer, D., and Löffler, J. F. (2011). Propagation dynamics of individual shear bands during inhomogeneous flow in a Zr-based bulk metallic glass. *Acta Materialia* **59**, 3205−3213.

146. Ai, K., and Dai, L. H. (2007). A new modified expanding cavity model for characterizing the spherical indentation behavior of bulk metallic glass with pile-up. *Scripta Materialia* **56**, 761−764.

147. Wei, B. C., Zhang, L. C., Zhang, T. H., Xing, D. M., Das, J., and Eckert, J. (2007). Strain rate dependence of plastic flow in Ce-based bulk metallic glass during nanoindentation. *Journal of Materials Research* **22**, 258−263.

148. Song, S. X., Wang, X.-L., and Nieh, T. G. (2010). Capturing shear band propagation in a Zr-based metallic glass using a high-speed camera. *Scripta Materialia* **62**, 847−850.

149. Klaumünzer, D., Maaβ, R., Dalla Torre, F. H., and Löffler, J. F. (2010). Temperature-dependent shear band dynamics in a Zr-based bulk metallic glass. *Applied Physics Letters* **96**, 061901.

150. Liu, Z. Y., Yang, Y., and Liu, C. T. (2011). Size-affected shear-band speed in bulk metallic glasses. *Applied Physics Letters* **99**, 171904.

151. Jiang, W. H., Liu, F. X., Liaw, P. K., and Choo, H. (2007). Shear strain in a shear band of a bulk-metallic glass in compression. *Applied Physics Letters* **90**, 181903.

152. Wright, W. J., Samale, M. W., Hufnagel, T. C., LeBlanc, M. M., and Florando, J. N. (2009). Studies of shear band velocity using spatially and temporally resolved measurements of strain during quasistatic compression of a bulk metallic glass. *Acta Materialia* **57**, 4639−4648.

153. Han, Z., Wu, W. F., Li, Y., Wei, Y. J., and Gao, H. J. (2009). An instability index of shear band for plasticity in metallic glasses. *Acta Materialia* **57**, 1367−1372.

154. Yang, Y., Ye, J. C., Lu, J., Liaw, P. K., and Liu, C. T. (2010). Characteristic length scales governing plasticity/brittleness of bulk metallic glasses at ambient temperature. *Applied Physics Letters* **96**, 011905.

155. Grady, D. E. (1992). Properties of an adiabatic shear-band process zone. *Journal of the Mechanics and Physics of Solids* **40**, 1197−1215.

156. Grady, D. E. (1994). Dissipation in adiabatic shear bands. *Mechanics of Materials* **17**, 289−293.

157. Grady, D. E., and Kipp, M. E. (1987). The growth of unstable thermoplastic shear with application to steady-wave shock compression in solids. *Journal of the Mechanics and Physics of Solids* **35**, 95−118.

158. Johnson, W. L., Lu, J., and Demetriou, M. D. (2002). Deformation and flow in bulk metallic glasses and deeply undercooled glass forming liquids − a self-consistent dynamic free volume model. *Intermetallics* **10**, 1039−1046.

159. Kim, J.-J., Choi, Y., Suresh, S., and Argon, A. S. (2002). Nanocrystallization during nanoindentation of a bulk amorphous metal alloy at room temperature. *Science* **295**, 654−657.

160. Flores, K. M., and Dauskardt, R. H. (2006). Mode II fracture behavior of a Zr-based bulk metallic glass. *Journal of the Mechanics and Physics of Solids* **54**, 2418−2435.

161. Xu, J., Ramamurty, U., and Ma, E. (2010). The fracture toughness of bulk metallic glasses. *Journal of the Minerals Metals and Materials Society* **62**, 10−18.

162. Molinari, A. (1997). Collective behavior and spacing of adiabatic shear bands. *Journal of the Mechanics and Physics of Solids* **45**, 1551−1575.

163. Zink, M., Samwer, K., Johnson, W. L., and Mayr, S. G. (2006). Plastic deformation of metallic glasses: Size of shear transformation zones from molecular dynamics simulations. *Physical Review B* **73**, 172203.

164. Francois, B., Lacombe, F., and Herrmann, H. J. (2002). Finite width of shear zones. *Physical Review E* **65**, 031311.

165. Dodd, B., and Bai, Y. L. (1985). Width of adiabatic shear bands. *Materials Science and Technology* **1**, 38−40.

166. Walley, S. M. (2007). Shear localization: A historical overview. *Metallurgical and Materials Transactions A* **38A**, 2629−2654.

167. Egami, T., Poon, S. J., Zhang, Z., and Keppens, V. (2007). Glass transition in metallic glasses: A microscopic model of topological fluctuations in the bonding network. *Pysical Review B* **76**, 024203.

168. Huang, Y. J., Shen, J., and Sun, J. F. (2007). Bulk metallic glasses: Smaller is softer. *Applied Physics Letters* **90**, 081919.

169. Liu, Y. H., Wang, G., Wang, R. J., Zhao, D. Q., Pan, M. X., and Wang, W. H. (2007). Super plastic bulk metallic glasses at room temperature. *Science* **315**, 1385−1388.

170. Das, J., Tang, M. B., Kim, K. B., Theissmann, R., Baier, F., Wang, W. H., and Eckert, J. (2005). 'Work-hardenable' ductile bulk metallic glass. *Physical Review Letters* **94**, 205501.

171. Conner, R. D., Johnson, W. L., Paton, N. E., and Nix, W. D. (2003). Shear bands and cracking of metallic glass plates in bending. *Journal of Applied Physics* **94**, 904−911.

172. Schroers, J., and Johnson, W. L. (2004). Ductile bulk metallic glass. *Physical Review Letters* **93**, 255506.

173. Ravichandran, G., and Molinari, A. (2005). Analysis of shear banding in metallic glasses under bending. *Acta Materialia* **53**, 4087−4095.

174. Chen, Y., Jiang, M. Q., and Dai, L. H. (2012). Collective behavior of shear bands in metallic glasses. Unpublished work.

175. Yu, G. S., Lin, J. G., Mo, M., Wang, X. F., Wang, F. H., and Wen, C. E. (2007). Effect of relaxation on pressure sensitivity index in a Zr-based metallic glass. *Materials Science and Engineering A* **460−461**, 58−62.

176. Dubach, A., Prasad, K. E., Raghavan, R., Löffler, J. F., Michler, J., and Ramamurty, U. (2009). Free-volume dependent pressure sensitivity of Zr-based bulk metallic glass. *Journal of Materials Research* **24**, 2697−2704.

177. Zhang, Z. F., Echert, J., and Schultz, L. (2003). Difference in compressive and tensile fracture mechanisms of Zr59Cu20Al10Ni8Ti3 bulk metallic glass. *Acta Materialia* **51**, 1167−1179.

178. Flores, K. M., and Dauskardt, R. H. (2001). Mean stress effects on flow localization and failure in a bulk metallic glass. *Acta Materialia* **49**, 2527−2537.

179. Lu, J., and Ravichandran, G. (2003). Pressure dependent flow behavior of Zr41.2Ti13.8Cu12.5Ni10Be22.5 bulk metallic glass. *Journal of Materials Research* **18**, 2039−2049.

180. Tandaiya, P., Ramamurty, U., and Narasimhan, R. (2009). Mixed mode (I and II) crack tip fields in bulk metallic glasses. *Journal of the Mechanics and Physics of Solids* **57**, 1880−1897.

181. Lund, A. C., and Schuh, C. A. (2003). Yield surface of a simulated metallic glass. *Acta Materialia* **51**, 5399−5411.

182. Schuh, C. A., and Lund, A. C. (2003). Atomistic basis for the plastic yield criterion of metallic glass. *Nature Materials* **2**, 449−452.

183. Sun, L., Jiang, M. Q., and Dai, L. H. (2010). Intrinsic correlation between dilatation and pressure sensitivity of plastic flow in metallic glasses. *Scripta Materialia* **63**, 943−946.

184. Shi, Y. F., and Falk, M. L. (2005). Strain localization and percolation of stable structure in amorphous solids. *Physical Review Letters* **95**, 095502.

185. Donohue, A., Spaepen, F., Hoagland, R. G., and Misra, A. (2007). Suppression of the shear band instability during plastic flow of nanometer-scale confined metallic glasses. *Applied Physics Letters* **91**, 241905.

186. Guo, H. (2007). Tensile ductility and necking of metallic glass. *Nature Materials* **6**, 735−739.

187. Jang, D., and Greer, J. R. (2010). Transition from a strong-yet-brittle to a stronger-and-ductile state by size reduction of metallic glasses. *Nature Materials* **9**, 215−219.

188. Liu, J. W., Cao, Q. P., Chen, L. Y., Wang, X. D., and Jiang, J. Z. (2010). Shear band evolution and hardness change in cold-rolled bulk metallic glasses. *Acta Materialia* **58**, 4827−4840.

189. Cao, Q. P., Liu, J. W., Yang, K. J., Xu, F., Yao, Z. Q., Minkow, A., Fecht, H. J., Ivanisenko, J., Chen, L. Y., Wang, X. D., Qu, S. X., and Jiang, J. Z. (2010). Effect of pre-existing shear bands on the tensile mechanical properties of a bulk metallic glass. *Acta Materialia* **58**, 1276−1292.

190. Li, W. H., Wei, B. C., Zhang, T. H., Xing, D. M., Zhang, L. C., and Wang, Y. R. (2007). Study of serrated flow and plastic deformation in metallic glasses through instrumented indentation. *Intermetallics* **15**, 706−710.

191. Wakeda, M., Shibutani, Y., Ogata, S., and Park, J. (2008). Multiple shear banding in a computational amorphous alloy model. *Applied Physics A* **91**, 281−285.

192. Sergueeva, A. V., Mara, N. A., Kuntz, J. D., Lavernia, E. J., and Mukherjee, A. K. (2005). Shear band formation and ductility in bulk metallic glasses. *Philosophical Magazine* **85**, 2671−2687.

193. Yokoyama, Y., Fujita, K., Yavari, A. R., and Inoue, A. (2009). Melleable hypoeutectic Zr−Ni−Cu−Al bulk glassy alloys with tensile plastic elongation at room temperature. *Philosophical Magazine Letters* **89**, 322−334.

194. Mukaia, T., Nieh, T. G., Kawamura, Y., Inoue, A., and Higashi, K. (2002). Effect of strain rate on compressive behavior of a Pd40Ni40P20 bulk metallic glass. *Intermetallics* **10**, 1071−1077.

195. Zhang, Y., Wang, W. H., and Greer, A. L. (2006). Making metallic glasses plastic by control of residual stress. *Nature Materials* **5**, 857−860.

196. Yu, H. B., Hu, J., Xia, X. X., Sun, B. A., Li, X. X., Wang, W. H., and Bai, H. Y. (2009). Stress-induced structural inhomogeneity and plasticity of bulk metallic glasses. *Scripta Materialia* **61**, 640−643.

197. Zhang, J. L., Yu, H. B., Lu, J. X., Bai, H. Y., and Shek, C. H. (2009). Enhancing plasticity of ZrTiCuNiBe bulk metallic glass by precompression. *Applied Physics Letters* **95**, 071906.

198. Yu, P., Bai, H. Y., Zhao, J. G., Jin, C. Q., and Wang, W. H. (2007). Pressure effects on mechanical properties of bulk metallic glass. *Applied Physics Letters* **90**, 051906.

199. Yu, P., Liu, Y. H., Wang, G., Bai, H. Y., and Wang, W. H. (2007). Enhance plasticity of bulk metallic glasses by geometric confinement. *Journal of Materials Research* **22**, 2384−2388.

200. Qiu, S. B., and Yao, K. F. (2008). Novel application of the electrodeposition on bulk metallic glasses. *Applied Surface Science* **255**, 3454−3458.

201. Chen, L. Y., Ge, Q., Qu, S., Jiang, Q. K., Nie, X. P., and Jiang, J. Z. (2008). Achieving large macroscopic compressive plastic deformation and work-hardening-like behavior in

a monolithic bulk metallic glass by tailoring stress distribution. *Applied Physics Letters* **92**, 211905.

202. Scudino, S., Surreddi, K. B., Wang, G., and Eckert, J. (2010). Enhanced plastic deformation of ZrTiCuNiBe bulk metallic glass by the optimization of frictional boundary restraints. *Scripta Materialia* **62**, 750−753.

203. Inoue, A., Katsuya, A., Amiya, K., and Masumoto, T. (1995). Preparation of amorphous Fe−Si−B and Co−Si−B alloy wires by a melt extraction method and their mechanical and magnetic properties. *Materials Transactions, JIM* **36**, 802−809.

204. Luo, J. H., Wu, F. F., Huang, J. Y., Wang, J. Q., and Mao, S. X. (2010). Superelongation and atomic chain formation in nanosized metallic glass. *Physical Review Letters* **104**, 215503, 4 pages.

205. Volkert, C. A., Donohue, A., and Spaepen, F. (2008). Effect of sample size on deformation in amorphous metals. *Journal of Applied Physics* **103**, 083539.

206. Wang, Y., Li, J., Hamza, A. V., and Barbee Jr., T. W. (2007). Ductile crystalline-amorphous nanolaminates. *Proceedings of the National Academy of Sciences* **104**, 11155−11160.

207. Lewandowski, J. J., Wang, W. H., and Greer, A. L. (2005). Intrinsic plasticity or brittleness of metallic glasses. *Philosophical Magazine Letters* **85**, 77−87.

208. Gu, X. J., Poon, S. J., Shiflet, G. J., and Lewandowski, J. J. (2009). Ductile-to-brittle transition in a Ti-based bulk metallic glass. *Scripta Materialia* **60**, 1027−1030.

209. Lewandowski, J. J., Gu, X. J., Nouri, A. S., Poon, S. J., and Shiflet, G. J. (2008). Tough Fe-based bulk metallic glasses. *Applied Physics Letters* **92**, 091918.

210. Cheng, Y. Q., Cao, A. J., and Ma, E. (2009). Correlation between the elastic modulus and the intrinsic plastic behavior of metallic glasses: The roles of atomic configuration and alloy composition. *Acta Materialia* **57**, 3253−3267.

211. Novikov, V. N., and Sokolov, A. P. (2004). Poisson's ratio and the fragility of glass-forming liquids. *Nature* **431**, 961−963.

212. Novikov, V. N., and Sokolov, A. P. (2006). Correlation of fragility and Poisson's ratio: Difference between metallic and nonmetallic glass formers. *Physical Review B* **74**, 064203.

213. Jiang, M. Q., and Dai, L. H. (2007). Intrinsic correlation between fragility and bulk modulus in metallic glasses. *Physical Review B* **76**, 054204.

214. Nemilov, S. V. (2007). Structural aspect of possible interrelation between fragility (length) of glass forming melts and Poisson's ratio of glasses. *Journal of Non-Crystalline Solids* **353**, 4613−4632.

215. Zhang, L., Cheng, Y. Q., Cao, A. J., Xu, J., and Ma, E. (2009). Bulk metallic glasses with large plasticity: Composition design from the structural perspective. *Acta Materialia* **57**, 1154−1164.

216. Jiang, M. Q., and Dai, L. H. (2010). Short-range-order effects on intrinsic plasticity of metallic glasses. *Philosophical Magazine Letters* **90**, 269−277.

217. Conner, R. D., Dandliker, R. B., Scruggs, V., and Johnson, W. L. (2000). Dynamic deformation behavior of tungsten-fiber/metallic glass matrix composites. *International Journal of Impact Engineering* **24**, 435−444.

218. Lee, S. B., Lee, K., Lee, S. K., and Lee, S. (2009). Compressive and tensile properties of STS304-continuous fiber-reinforced Zr-based amorphous alloy matrix composite fabricated by liquid pressing process. *Metallurgical and Materials Transactions A* **40A**, 3159−3170.

219. Zhang, H. F., Li, H., Wang, A. M., Fu, H. M., Ding, B. Z., and Hu, Z. Q. (2009). Synthesis and characteristics of 80 vol.% tungsten (W) fibre/Zr based metallic glass composite. *Intermetallics* **17**, 1070−1077.

220. Liu, J. M., Zhang, H. F., Yuan, X. G., Fu, H. M., and Hu, Z. Q. (2011). Synthesis and properties of carbon short fiber reinforced ZrCuNiAl metallic glass matrix composite. *Materials Transactions* **52**, 412−415.

221. Zong, H. T., Ma, M. Z., Liu, L., Zhang, X. Y., Bai, B. W., Yu, P. F., Qi, L., Jing, Q., Li, G., and Liu, R. P. (2010). W(f)/Zr(41.2)Ti(13.8)Cu(12.5)Ni(10)Be(22.5) bulk metallic glass composites prepared by a new melt infiltrating method. *Journal of Alloys and Compounds* **504**, S106−S109.

222. Eckert, J., Das, J., Pauly, S., and Duhamel, C. (2007). Mechanical properties of bulk metallic glasses and composites. *Journal of Materials Research* **22**, 285−301.

223. Hofmann, D. C., Suh, J. Y., Wiest, A., Duan, G., Lind, M. L., Demetriou, M. D., and Johnson, W. L. (2008). Designing metallic glass matrix composites with high toughness and tensile ductility. *Nature* **451**, 1085−1089.

224. Pauly, S., Gorantla, S., Wang, G., Kühn, U., and Eckert, J. (2010). Transformation-mediated ductility in CuZr-based bulk metallic glasses. *Nature Materials* **9**, 473−477.

225. Liu, J. M., Zhang, H. F., Fu, H. M., Hu, Z. Q., and Yuan, X. G. (2010). In situ spherical B2 CuZr phase reinforced ZrCuNiAlNb bulk metallic glass matrix composite. *Journal of Materials Research* **25**, 1159−1163.

226. Qiao, J. W., Sun, A. C., Huang, E. W., Zhang, Y., Liaw, P. K., and Chuang, C. P. (2011). Tensile deformation micromechanisms for bulk metallic glass matrix composites: From work-hardening to softening. *Acta Materialia* **59**, 4126−4137.

227. Deng, S. T., Diao, H., Chen, Y. L., Yan, C., Zhang, H. F., Wang, A. M., and Hu, Z. Q. (2011). Metallic glass fiber-reinforced Zr-based bulk metallic glass. *Scripta Materialia* **64**, 85−88.

228. Ma, W. F., Kou, H. C., Chen, C. S., Li, J. S., Chang, H., Zhou, L., and Fu, H. Z. (2008). Compressive deformation behaviors of tungsten fiber reinforced Zr-based metallic glass composites. *Materials Science and Engineering A* **486**, 308−312.

229. Qiu, K. Q., Suo, Z. Y., Ren, Y. L., and Yu, B. (2007). Observation of shear bands formation on tungsten fiber-reinforced Zr-based bulk metallic glass matrix composite. *Journal of Materials Research* **22**, 551−554.

230. Li, H., Subhash, G., Kecskes, L. J., and Dowding, R. J. (2005). Mechanical behavior of tungsten preform reinforced bulk metallic glass composites. *Materials Science and Engineering A* **403**, 134−143.

231. Wang, G., Chen, D. M., Shen, J., Stachurski, Z. H., Qin, Q. H., Sun, J. F., and Zhou, B. D. (2006). Deformation behaviors of a tungsten-wire/bulk metallic glass matrix composite in a wide strain rate range. *Journal of Non-Crystalline Solids* **352**, 3872−3878.

232. Jiao, T., Kecskes, L. J., Hufnagel, T. C., and Ramesh, K. T. (2004). Deformation and failure of Zr(57)Nb(5)Al(10)Cu(15.4)Ni(12.6)/W particle composites under quasi-static and dynamic compression. *Metallurgical and Materials Transactions A* **35A**, 3439−3444.

233. Hays, C. C., Kim, C. P., and Johnson, W. L. (2000). Microstructure controlled shear band pattern formation and enhanced plasticity of bulk metallic glasses containing in situ formed ductile phase dendrite dispersions. *Physical Review Letters* **84**, 2901−2904.

234. Qiao, J. W., Wang, S., Zhang, Y., Liaw, P. K., and Chen, G. L. (2009). Large plasticity and tensile necking of Zr-based bulk-metallic−glass-matrix composites synthesized by the Bridgman solidification. *Applied Physics Letters* **94**, 151905.

235. Wu, Y., Xiao, Y. H., Chen, G. L., Liu, C. T., and Lu, Z. P. (2010). Bulk metallic glass composites with transformation-mediated work-hardening and ductility. *Advanced Materials* **22**, 2770−2773.
236. Matsumoto, N., Matsumoto, R., and Miyazaki, N. (2009). Estimation of shear-banding resistance in metallic glass containing nano-crystalline particles. *Journal of Non-Crystalline Solids* **355**, 29−32.
237. Abdeljawad, F., and Haataja, M. (2010). Continuum modeling of bulk metallic glasses and composites. *Physical Review Letters* **105**, 125503.